Federal University of Rio de Janeiro

Graduate Program in Engineering of Chemical and Biochemical Processes

THERMODYNAMIC PROPERTIES OF $CH_4 + CO_2$ AND $CH_4 + N_2$ BINARY MIXTURES CONFINED IN BARITE, CALCITE AND MONTMORILLONITE NANOPORES BY MOLECULAR DYNAMICS

Yamara Matos Oliveira

Master's thesis presented to the Graduate Program in Engineering of Chemical and Biochemical Processes, from the School of Chemistry of the Federal University of Rio de Janeiro, as partial fulfillment of the requirements for the degree of Mestre em Ciências em Engenharia de Processos Químicos e Bioquímicos.

Advisors: Charlles Rubber de Almeida Abreu
Frederico Wanderley Tavares

Rio de Janeiro

October, 2019

THERMODYNAMIC PROPERTIES OF CH_4 + CO_2 AND CH_4 + N_2 BINARY MIXTURES CONFINED IN BARITE, CALCITE AND MONTMORILLONITE NANOPORES BY MOLECULAR DYNAMICS

Yamara Matos Oliveira

Master's thesis submitted to the faculty body of the Graduate Program in Engineering of Chemical and Biochemical Process (EPQB) from the School of Chemistry (EQ) of the Federal University of Rio de Janeiro (UFRJ), as partial fulfillment of the requirements for the degree of Mestre em Ciências em Engenharia de Processos Químicos e Bioquímicos.

Approved by:

_____
Prof. Charlles Rubber de Almeida Abreu, D.Sc. – EPQB/EQ/UFRJ

_____
Prof. Frederico Wanderley Tavares, D.Sc. – PEQ/COPPE/UFRJ

_____
Prof. Carla Luciane Manske Camargo, D.Sc. – EPQB/EQ/UFRJ

_____
Prof. Luciano Tavares da Costa, D.Sc. – PPGQ/UFF

RIO DE JANEIRO, RJ – BRAZIL
OCTOBER, 2019

Acknowledgements

Apesar do inglês ser uma língua prática e ideal para textos técnicos, não supera ao português na hora de tratar de sentimentos. Dessa forma, peço licença, pois me farei um carinho e escreverei esta parte em minha língua materna. Parte esta que, para mim, de todo o texto, é a mais importante, pois agradecer é reconhecer que eu nada fiz sozinha. Particularmente, durante o mestrado, esse foi o meu maior aprendizado. Agradeço a Deus, verdadeiro amado de minh' alma e sentido da minha vida, reconheço que sem Ti eu nada seria. A Nossa Senhora, pela delicadeza nas pequenas demonstrações de amor no meu dia a dia e por ser presença constante.

Obrigada aos meus pais e a minha irmã por todo apoio e por acreditarem no poder transformador da educação. Também agradeço a toda minha família pelas orações e torcida. Ao amor da minha vida, Girlano, por sempre dizer "vai, Yah, você consegue, nós damos um jeito!", você é a pessoa mais incrível que conheci e uma das minhas maiores inspirações.

Agradeço também a todos os meus amigos de infância e adolescência, vocês são responsáveis por minhas melhores e mais doces lembranças. Obrigada ao Escalada e ao GJS por estarem juntos comigo na caminhada da fé, por toda acolhida e aceitação e por me ajudarem a vencer meus medos. Desses grupos surgiram amizades que sei que vão transcender a morte.

Agradeço profundamente aos meus professores orientadores, Charlles e Frederico, pela paciência e cuidado ao lidarem comigo. Charlles em especial agradeço por ser objeto de minha profunda admiração devido à inteligência e integridade. Frederico, obrigada por ser testemunho de felicidade ao seguir verdadeiramente sua vocação.

À família ATOMS, obrigada por serem o melhor conjunto de indivíduos que cruzaram a minha vida. Eu sou completamente apaixonada por esse laboratório e isso é por causa de todos que dele fazem parte. Em especial, agradeço ao Marlon e ao Thiago, vocês basicamente me sustentaram durante esse período e eu sou muito grata pela confiança, carinho e amor partilhados, amo vocês! Obrigada também ao comunidança e às minhas alunas de dança do ventre, vocês foram as melhores coisas que me aconteceram esse ano.

Por fim, agradeço a todos que de alguma forma contribuíram para que eu chegasse até aqui. Obrigada!

"Por revelação me foi dado a conhecer o mistério."

São Paulo

Resumo da Dissertação apresentada ao EPQB/UFRJ como parte dos requisitos necessários para a obtenção do grau de Mestre em Ciências (M.Sc.)

PROPRIEDADES TERMODINÂMICAS DE MISTURAS BINÁRIAS DE CH_4 + CO_2 E CH_4 + N_2 CONFINADAS EM NANOPORES DE BARITA, CALCITA E MONTMORILONITA POR DINÂMICA MOLECULAR

Yamara Matos Oliveira

Outubro/2019

Advisors: Charlles Rubber de Almeida Abreu
         Frederico Wanderley Tavares

Program: Engenharia de Processos Químicos e Bioquímicos

Neste trabalho, estuda-se a diferença no comportamento do metano, dióxido de carbono e nitrogênio em nanoporos de montmorilonita (argila), barita (sulfato insolúvel em água) e calcita (carbonato de cálcio), e misturas binárias de metano e dióxido de carbono e metano e nitrogênio nesses sólidos pela dinâmica molecular. Devido às interações parede-fluido, as propriedades do fluido confinado podem variar drasticamente quando comparadas às do mesmo fluido em fase volumar. Quanto menor o tamanho do poro (portanto, quanto maior o confinamento), mais intensos são os efeitos observados. Os fluidos em nanoporos geralmente não são homogêneos na direção perpendicular à interface entre o sólido e fluido – na qual são observados fenômenos de adsorção e/ou empacotamento. Nos modelos de campo de força utilizados neste trabalho, as moléculas são rígidas e, portanto, as interações são calculadas apenas pelas forças de Van der Waals e eletrostática. As simulações foram realizadas com poros do tipo fenda (placas paralelas) e testadas duas distâncias diferentes e duas temperaturas para cada mistura binária. A existência de reservatórios de óleo e gás no Brasil com altos níveis de CO_2 (pré-sal) e N_2 (Urucu) mostra a necessidade de métodos alternativos de separação para esses gases contaminantes, tanto em termos de redução de poluentes quanto em termos de maior valor agregado do óleo e/ou do gás natural. Mostra-se, através da análise do perfil de densidade nos nanoporos, que as interações parede-fluido e o grau de confinamento podem induzir a separação dos componentes.

Abstract of Master's thesis presented to EPQB/UFRJ as a partial fulfillment of the requirements for the degree of Master of Science (M.Sc.)

THERMODYNAMIC PROPERTIES OF CH_4 + CO_2 AND CH_4 + N_2 BINARY MIXTURES CONFINED IN BARITE, CALCITE AND MONTMORILLONITE NANOPORES BY MOLECULAR DYNAMICS

Yamara Matos Oliveira

October/2019

Advisors: Charlles Rubber de Almeida Abreu
           Frederico Wanderley Tavares

Graduate Program: Engineering of Chemical and Biochemical Processes

In this work, we study the difference in the behavior of methane, carbon dioxide and nitrogen in montmorillonite (clay), barite (non-water-soluble sulfate) and calcite (calcium carbonate) nanopores, and binary mixtures of methane and carbon dioxide and methane and nitrogen in such solids by molecular dynamics. Due to fluid-wall interactions, confined fluid properties can vary drastically when compared to those of the same fluid as a bulk phase. The smaller the pore size (hence the greater the confinement), the more intense are the observed effects. Fluids in nanopores are usually inhomogeneous in the direction perpendicular to the fluid-wall interface – in which adsorption and/or packing phenomena are observed. In the chosen force-field models, the molecules are rigid and therefore the interactions are calculated only by the van der Waals and electrostatic forces. The behavior of the fluid inside slit-like pores (parallel plates) was simulated, and two different distances and two temperatures were tested for each binary mixture. The existence in Brazil of oil and gas reservoirs with high levels of CO_2 (pre-salt) and N_2 (Urucu) shows the need for alternative methods of separation for these contaminating gases, both in terms of reducing pollutants and in terms of increasing the value added to oil and/or natural gas. It is shown, through analysis of the density profile within the nanopores, that the fluid-wall interactions and the degree of confinement can induce the separation of the components.

Contents

List of Figures

List of Tables

List of Symbols

θ_o equilibrium value of the angle, p. 34

k_{angle} angle constant, p. 34

k_{bond} bond constant, p. 34

E   total energy, p. 14

K   kinetic energy, p. 14

U   interaction potential, p. 14

$\boldsymbol{F}$ (t)   force exerted on the particle, p. 14

$\boldsymbol{r^N}$ particles positions, p. 14

ϵ potential well depth, p. 26

σ related to the atomic diameters, p. 26

q   charge, p. 34

List of Abbreviations

ANP   National Agency of Petroleum, Natural Gas and Biofuels, p. 1

Chapter 1

Introduction

In Brazil, the number of proven natural gas reserves increased significantly between 2008 and 2017, by 11.52%. This is in line with the increase in oil reserves. This growth is mainly due to gas in associated form inside the reservoirs (MINISTÉRIO DE MINAS E ENERGIA [1]). In addition, there has also been a significant increase in natural gas production, consumption and sale in the country in recent years. Figure 1.1 shows the evolution of natural gas production in Brazil between 2008 and 2017 (ANP [10]). It can be noted that gas production between these years almost doubled, and one of the main reasons that explains this fact is the start of gas production in the pre-salt area. Pre-salt reservoir fields increased natural gas production from a daily average of 2.03 million m^3 in 2010 to 49.80 million m^3 in 2017 (ANP [10]MINISTÉRIO DE MINAS E ENERGIA [1]).

From 2008 to 2017, it is also possible to observe Figure 1.2 that there was a lot of investment to increase the processing capacity of some large poles in the country, such as Urucu and Caraguatuba (ANP [2]).

It is worth noticing here that one of the characteristics of the natural gas found in the pre-salt is the high carbon dioxide content and one of the great challenges of the Urucu processing pole is to working with the high amounts of nitrogen found in the natural gas processed at the site (ANP [10]). To be available for consumption, natural gas must meet certain specifications. The National Agency of Petroleum, Natural Gas and Biofuels (ANP) regulates the natural gas processed and imported in Brazil (ANP [11]). Under ANP regulation, the inert gas limit (CO_2 + N_2) for the South, Southeast and Midwest Regions is 6%. For the Northeast Region, on its

turn, it is 8% while for the North Region, 18% (ANP [11]).
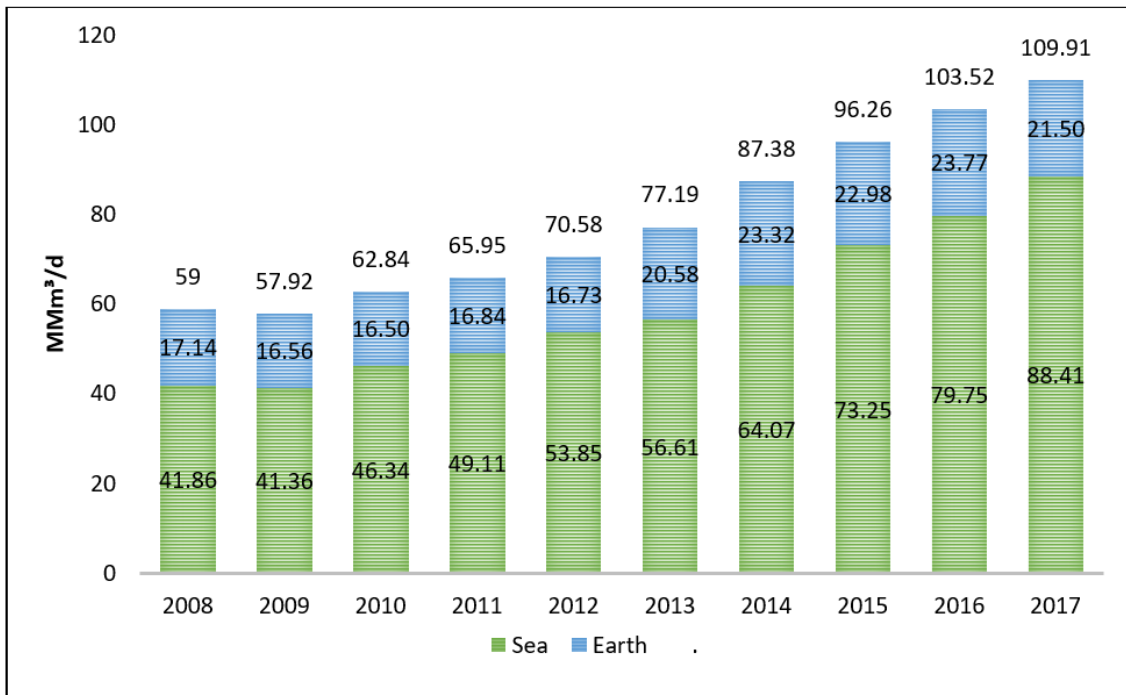
Figure 1.1: Natural gas production in Brazil from 2008 to 2017. Adapted from MINISTÉRIO DE MINAS E ENERGIA [1]
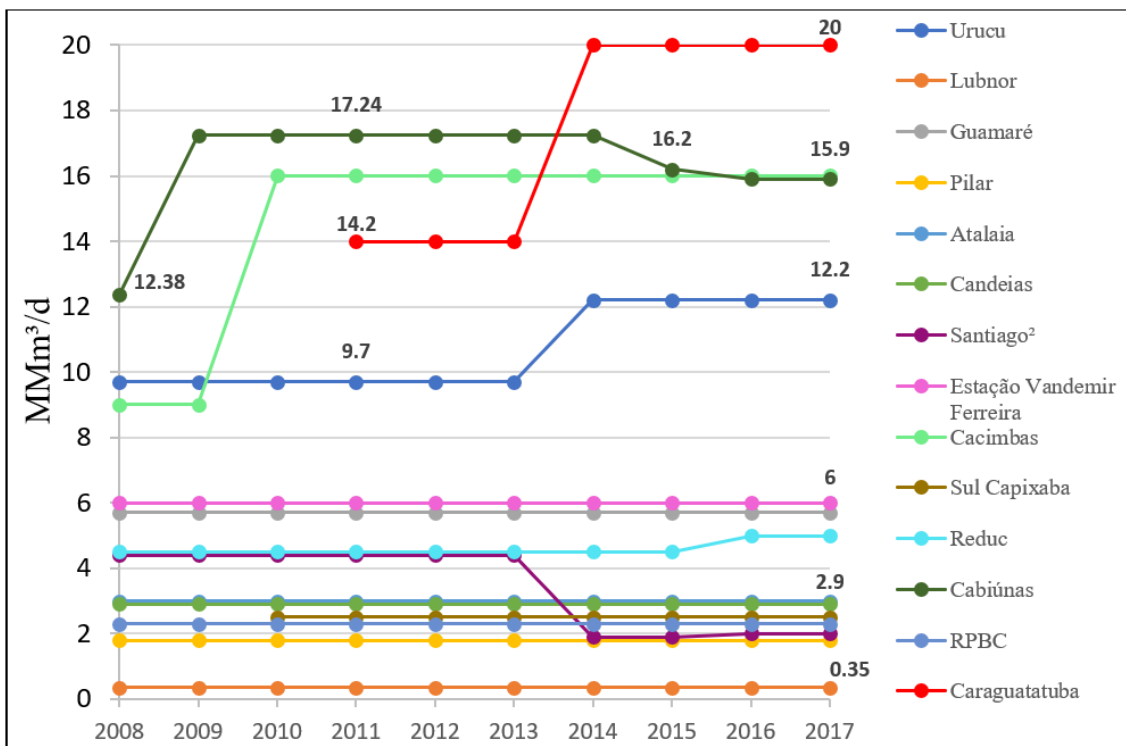
Figure 1.2: Evolution of natural gas processing capacity, by producing poles - 2008-2017. Adapted from ANP [2]

As the numbers show, there is still a high price concession for both the North

2

and Northeast regions. There is a tendency to reduce this type of concession due to ongoing changes in environmental regulations in order to make them more restrictive, to reduce impacts on the environment.This is a worldwide movement of which Brazil is a main actor, being a major exporter of the natural gas and oil industry (KIDNAY *et al.* [12]).The vast majority of international organs that regulate the presence of inert gases (CO_2 + N_2) in natural gas stipulate a maximum of 4% (KIDNAY *et al.* [12]). Therefore, Brazil, as aforementioned, still lags behind in this regard.

It is also noteworthy that the carbon dioxide problem goes further as it is a greenhouse gas (SANTOS *et al.* [13]). This subject has been the target of great worldwide repercussion and tends to generate discussions to further control the dispersion of said gas in the atmosphere. To address these challenges, there are some well-established techniques in the processing industry that promote the separation of carbon dioxide and nitrogen from natural gas. The most conventional process used to remove CO_2 from natural gas is the use of large adsorption and regeneration towers with a water based amine solution (RUFFORD *et al.* [3], KIDNAY *et al.* [12]). Capital investment, operating and maintenance costs to implement this method are considered high.

In addition to the problem of amine solution regeneration, there is also the issue of its disposal. When it comes to offshore production, there is another additional problem: it is necessary to dehydrate the gas before it gets sent to the processing units to avoid hydrate formation (KIDNAY *et al.* [12]). However, the conventional CO_2 removal process saturates natural gas with water vapor and it is necessary to duplicate existing dehydration equipment, which requires a large financial investment. For N_2 removal, the most common process is cryogenic distillation, which is considered quite expensive (KIDNAY *et al.* [12]).

Often the high investment costs in these types of techniques do not justify the manipulation of certain high inert gas reserves. However, finding techniques that are less costly may make these reserves' exploitation feasible.

When trying to find new processes, it is necessary to understand the possible mechanisms that may promote the separation of these components from natural gas. These mechanisms are intrinsically related to differences in mixture component, and these differences may be related to thermodynamic properties or transport proper-

ties, some of them shown in Table 1.1 (RUFFORD *et al.* [3], RUTHVEN [14]).

Table 1.1: Molecular, thermodynamic and transport properties of methane, carbon dioxide, nitrogen (RUFFORD *et al.* [3]).

Property	CH_4	CO_2	N_2
Kinetic diameter (Å)	3.8	3.3	3.64
Normal boiling point (NBP) (K)	111.7	-	77.3
Critical temperature (K)	3.8	304.1	126.2
Critical pressure (kPa)	4600	7380	3400
$_{vap}$ at NBP (kJ/mol)	8.17	26.1	5.58
Polarizability (Å^3)	2.448	2.507	1.71
Quadrupole moment (DÅ)	0.02	4.3	1.54

These differences may guide the type of separation process that can be used and new processes which can be studied from this data. Separation techniques include adsorption, absorption, cryogenic distillation and membrane technologies (RUFFORD *et al.* [3]). As an alternative to solvent processes in the early 1990s, adsorptive processors began to be considered. Adsorption is a relatively easy and economical technique when compared to the other mentioned techniques. Among its advantages there is the reduced use of energy for regeneration, and, also, the fact that it may have a greater separation capacity and greater selectivity (RITTER and EBNER [15], TAGLIABUE *et al.* [16]). In recent decades, great efforts have been made to study and develop this technology. The cyclic adsorption process usually includes pressure or vacuum swing adsorption (PSA / VSA) and temperature swing adsorption (TSA) (RITTER and EBNER [15]). Adsorption on porous solid media using pressure and/or temperature swing approaches is an emerging alternative that seeks to reduce costs. Adsorption can achieve separation of the mixture through the use of one of the three following mechanisms (RUTHVEN [14]):

- Through differences in fluid / wall interaction after thermodynamic equilibrium.
- Through differences in the size of mixtures molecules.
- Through differences in pore diffusion rates.

One of the most important parts of these processes, if not the most important, is the selection of the adsorbent for the mixture to be separated, which in this case

are CO_2 and N_2 from CH_4 (RUFFORD *et al.* [3], BAGHERINIA and SHADMAN [17]). These three compounds have similar sizes and this feature makes it difficult to separate them by diameter differences. Carbon dioxide has a high quadrupolar moment, which means it can be more attracted to an electric field gradient than N_2 and CH_4 (RUTHVEN [14]).

There are some materials that have been reported in the literature with some selectivity for CO_2 and N_2 in mixtures with CH_4 such as Cu – MOF and small pore zeolites, such as clinoptilolite (RUFFORD *et al.* [3]). To verify this selectivity, the most common methodology known in the literature is the construction of adsorption isotherms (RITTER and EBNER [15], EBNER and RITTER [18]). The adsorption isotherm is the equilibrium relationship between the concentration in the fluid phase and the concentration in the adsorbent particles at a given temperature. For gases, this measurement is usually given as a percentage of mol or as partial pressure. For liquids, it is usually given in units of mass. For the construction of this isotherm the most accepted methodologies are still the experimental ones. However, the high costs of equipment justify the great efforts to look for alternative methodologies that can yield reliable results and do not involve a high investment in research (FARAMAWY *et al.* [19]).

Thus, a great effort has been exerted in trying to understand these processes with minimal experimental data (RUFFORD *et al.* [3]). In this direction, there are modeling and simulation tools that come as theoretical studies and offer solution through models and numerical calculations. One such tool is molecular dynamics that is based on force field models, which are models with few parameters (decrease errors) and are able to provide responses in conditions far from what they were originally parameterized.

Molecular dynamics is a computational simulation method that studies the motion of particles on the nanometer scale over time (TUCKERMAN [20]). These molecules interact with each other according to a given interaction potential. The equations of motion are solved given the initial conditions of the simulation. After reaching thermodynamic equilibrium, it is possible to perform calculations by means of the temporal averages of particle positions. By correlations, it is possible to make the connection between the microscopic and the macroscopic state (TUCKERMAN

[20], THOMPSON [21]) However, in this work we are specifically interested in the microscopic scale, as we are looking to describe the behavior inside the adsorbent pore, which is in the few nanometer scale. Our goal is to enter a field of study that is still recent and needs discussion, which is this segment of the application of molecular dynamics to nanoscale confined fluids.

A recently published literature review article discusses the challenges and differences observed in this type of simulation (THOMPSON [21]). The smaller the pore size, the more fluid molecules are influenced by their interactions with the pore walls. Thus, it can be observed that up to more than half of the fluid molecules may be forming a layer at the wall interface. Because of these interactions, fluid properties can change dramatically when compared with the fluid in the bulk phase (CYGAN *et al.* [4], SANTOS *et al.* [13], THOMPSON [21]). These changes are often not intuitive and require further study. Several variables can be influential in changing the dynamics with the wall such as pore size, wall type, wall geometry, etc (PATHAK *et al.* [22]). It is reported in the literature that packaging is dominated by steric effects and the shape of the fluid particle orienting itself is highly included by electrostatic interactions. Loughnane *et al.* (1999) [23] reported, in his work, that he believed that hydrogen bonds were responsible for orientation with the wall. However, later in 2009, Morales *et al.* [24] noted that they were not necessary for the effect to be observed but could increase this effect.

Confined fluids investigated via molecular dynamics is, notably, still an area that needs study, but significant and positive advances have already been made confirming experimental data (THOMPSON [21]). By studying the dynamics of the fluid/wall interaction, it is possible to verify the differences in these interactions with different types of walls and to observe if it is possible to promote the separation of the components of the fluid mixture inside the solid.

In this work three porous rocks are studied by molecular dynamics in order to better understand their affinity with three components present in the sub-quality natural gas: methane, carbon dioxide and nitrogen and their binary mixtures.

1.1 Motivations

The scenario of natural gas production and consumption in Brazil, in its continuous growth, justifies investments in new separation processes. The goal is to to meet the increasingly restrictive environmental standards that regulate the production and commercialization of natural gas. Also make sub-quality natural gas fields a viable exploration alternative.

Although there are already several studies in the development of separation process development and discovery of new adsorbents, molecular dynamics has become an interesting methodology to understand certain interaction phenomena inside the adsorbent pores which are normally challenging to be studied experimentally.

Preliminary simulation studies can guide investments in experimental studies by providing information on the behavior of fluids inside solid structure. Thus, it is interesting to validate molecular simulation methodologies that can contribute to experimental studies of new adsorbents.

1.2 Objectives

The main goal of this study is to investigate how molecular dynamics can be an aid in understanding nanoscale environments, specifically inside pores of solid materials. By analyzing the pore density profiles of mixtures of carbon dioxide and methane, and nitrogen and methane inside three different solid structures (calcite, barite, and montmorillonite), a greater understanding of how fluid/wall interactions can assist in the separation of these mixtures is expected.

This study also aims at determining which of these solids has the ability to better separate the binary mixtures presented, as well as to analyze the effect of pore size and temperature on the dynamics with the interface.

Specifically, we aim to:

- Assemble nanoscale solid crystals from unit cell models.

- Test solid integrity during long molecular dynamics simulations.

- Assemble simulation boxes with solid crystals and binary mixtures of CO_2 + CH_4 and N_2 + CH_4 and their respective pure compounds.

- Simulate binary mixtures between slit-like pores (parallel plates) of three dif-

7

ferent solid types at different distances and temperatures

- Observe the change in wall adsorption the behavior of mixtures when compared to pure substances.

- Determine which solids can promote separation of the studied mixtures.

1.3   Organization of the Dissertation

This document consists of 6 additional chapters. Chapter 2 presents the literature review on the current scenario of MD as a technology to study confined fluid and simulations technique to study methane, carbon dioxide and nitrogen.

Chapter 3 is a summary of the main concepts of statistical thermodynamics and molecular simulation and some solution algorithms for such problems. The details of the methodology used in this work will be described in Chapter 4, while Chapter 5 will be devoted to the presentation of the results obtained from the methods developed in the previous chapter, under different conditions of temperature, adsorbent type, and pore sizes. The conclusions and suggestions for future work are in Chapter 6 and References are in Chapter 7.

Chapter 2

Literature Review

2.1 Molecular Dynamics Simulations Applied to Confined Fluids

In recent years, the scientific community has made many efforts to better understand the fluid in confinement by using molecular dynamics approaches. Wang *et al.* (2018) [25] conducted a series of molecular dynamics simulations to study the diffusion process of supercritical methane in shale nanopores, in order to evaluate the effects of pore pressure, pore size, and the moisture content in different mineral matrix types. Their results showed an anisotropic diffusion behavior in both perpendicular and parallel directions in relation to the mineral surface. Also, they realized that an increase in pore size and in temperature make the confined methane molecules diffuse faster, but the diffusion is hindered by an increase in pressure (WANG *et al.* [25]).

Wang *et al.* (2016) [26] studied the behavior of octane and supercritical carbon dioxide confined in slit-shaped organic nanopores. By analyzing the density profile of the simulation box, they observed the layering structure in the interface and the preferential adsorption of CO_2 relative to C_8H_{18} and CH_4. They also calculated the velocity profiles over the pore by imposing a constant velocity on the wall. This hydrodynamic study showed that organic slit pores tends to provide plug-like velocity profiles, which is an interesting new behavior when compared with the well-known parabolic profile observed in inorganic nanopores (WANG *et al.* [26]).

Le *et al.* (2015) [27] studied pure n-butane and mixtures containing n-butane and carbon dioxide confined in wide slit-shaped pores carved out of cristobalite silica. They observed a relation between the quantity of hydroxyl groups on the surface and the preferential adsorption of carbon dioxide near this groups. From their results, they showed that the presence of CO_2 enhances the n-butane mobility because of the preferential CO_2 adsorption inside the pore walls (LE *et al.* [27]).

In 2017, Le *et al.* (2017) [28] studied systems composed of propane and water confined inside cylindrical pores carved out of amorphous silica. They analyzed the diffusivity of propane in the cylinder according to the pressure and to the amount of water, showing that the formation of water bridges across the silica pores hinders the propane self-diffusion. They also quantified the residence time of water molecules in the silica pore, the lifespan of the hydrogen bonds and the rotational diffusion in the cylindrical pores (LE *et al.* [28]).

Franco *et al.* (2016)[29] investigated methane, nitrogen, and carbon dioxide confined between two calcite crystal planes. They calculated parallel self-diffusion coefficients and concluded that the molecules close to the calcite surface tend to diffuse differently over different directions. They also investigated the behavior of the self-diffusion coefficient at different temperatures and calcite pore sizes (FRANCO *et al.* [29]).

2.2 Adsorption of carbon dioxide, methane and nitrogen

In the scope of the compounds that will be studied in this work, in recent years, many researchers have studied CO_2, CH_4 and N_2 adsorption, by both theoretical and experimental ways.

Karra and Walton *et al.* (2010) [30] studied systems of CO_2, CO and N_2 confined in Metal Organic Fremeworks (MOFs) by grand canonical Monte-Carlo simulations. They analyzed the effect of pore size, heat of adsorption, and other variables on the adsorption of these three compounds for different MOFs (KARRA and WALTON [30]).

Mishra *et al.*(2012) [31] investigated the adsorption properties of confined CO_2,

CH_4 and N_2 inside a zinc-based MOF via the Ideal Adsorbed Solution Theory. They reported the behavior of binary mixtures inside the pore and predicted their selectivity, showing that CO_2 molecules preferentially adsorbs in the studied matrix over the methane and nitrogen. They also showed that there is an explicit relation between selectivity, pressure and composition of the mixture (MISHRA *et al.* [31]).

In another work, Zhang *et al.* (2012) [32] presented experimental and computational results that suggests that Cu-TDPAT is a promising material that can favor the separation of CO_2 from N_2 and CH_4 (ZHANG *et al.* [32]).

Likewise, Yi *et al.* (2013) [33] did a series of experiments to study CO_2, CH_4 and N_2 adsorption equilibrium isotherms on microwave-activated carbon. They also concluded that CO2 dominates the adsorption in the system (YI *et al.* [33]).

Billemont *et al.* (2013) [34] investigated, via experiments and molecular simulations, the adsorption of CO_2 and CH_4 in carbons nanoporous in the presence of water. They showed by both approaches that, for small amounts of adsorbed water, the shape of the adsorption isotherms remains similar, but it is possible to show a slight decrease in the CO_2 and CH_4 adsorption. In the other hand, only experiments showed the formation of methane or carbon dioxide clathrates for large amounts of adsorbed water (BILLEMONT *et al.* [34]).

In 2014, Bagherinia et al. (2014) [17] studied CO_2, CH_4 and N_2 interactions with a single-walled silicon carbon nanotubes by grand canonical Monte-Carlo simulations. Their results demonstrate that, under 25 °C and high pressure, the CO2 also dominates the adsorption in the system, followed by CH_4 and then N_2. They also calculated the isosteric heat of adsorption for these gases (BAGHERINIA and SHADMAN [17]).

More recently, in 2016, Akbarzadeh *et al.* [35] studied by MD simulations the adsorption behaviors of methane and carbon dioxide in silicon carbide nanotubes and in carbon nanotubes. As in the previous studies discussed here, they showed that carbon dioxide dominates the adsorption in the system over the methane (AKBARZADEH and ABBASPOUR [35]).

In 2017, Dang *et al..* (2017) [36] investigated mixtures of co_2 and ch_4 confined inside brown coal. They used three types of computational simulation methodology: grand canonical Monte Carlo (GCMC), MD and density functional theory (DFT)

simulations. They analyzed the adsorption behavior of these two components at two different temperatures and in a defined pressure range. They showed that the co_2 adsorption is largely influenced by the basicity of the oxygen- and the nitrogen-containing groups, and also discussed that the polarity is a decisive factor for the adsorption in sulfur functional groups (DANG *et al.* [36]).

2.3   Final Considerations

Based on what has been presented, it can be noted that a great effort has been made to better understand the effects of confinement in various types of substances and how this effect may influence the separation of mixtures. Several techniques are applied, but it is possible to notice the significant increase over the years of studies that use the computer simulation as methodology. Several proposals have been presented for adsorption of co_2 mixtures; however, the literature still does not show good results for the favorable selectivity to n_2

As relatively new study options for adsorbents, there are clays that are abundant and inexpensive materials and once used for they can be buried instead of having to undergo a regeneration process (BACSIK *et al.* [37]).

The calcite, that is present in shale gas reservoirs and has already been shown favorable to be applied for carbon sequestration (SANTOS *et al.* [13], FRANCO *et al.* [29]).

As well as barite which is a cheap mineral that is already very common in the use of the oil industry in drilling muds (BLEIWAS and MILLER [38])

These three solids are studied here to observe the behavior of the $ch_4 + co_2$ and $ch_4 + n_2$ mixtures confined in their pores using molecular dynamics. As discussed earlier, both nitrogen and carbon dioxide are considered contaminants in the production of natural gas. It is, therefore, important to study the separation techniques of these components in mixtures containing light hydrocarbons. Molecular dynamics (MD) has been shown to be a powerful tool in the study of phenomena at the nanometric scale, for example, inside the pore of rocks. Molecular dynamics has been remarkably successful in its ability to predict macroscopic thermodynamic and dynamic observables for a wide variety of systems using the rules of classical

statistical mechanics (TUCKERMAN [20]). MD is continually growing as an option for describing system properties under conditions that experimental predictions are difficult to acquire.

Chapter 3

Computational Methods

3.1 Molecular Dynamics

3.1.1 Introduction

Molecular dynamics a numerical simulation technique for computing the equilibrium and transport properties of a classical many body system in which the temporal evolution of a set of interacting particles is followed by integrating their equations of motion. In this context, the word classical means that it uses the laws of classical mechanics (TUCKERMAN [20]), notably Newton's equations, which for each particle i of mass m_i are written:

$$
m_i \frac{d^2 \boldsymbol{r_i}(t)}{dt^2} = \boldsymbol{F_i}(t)
$$
$$
\boldsymbol{F_i}(t) = -\frac{\partial U(\boldsymbol{r^N})}{\partial \boldsymbol{r_i}} \ with \ \frac{\partial}{\partial \boldsymbol{r}} : gradient \ operator. \tag{3.1}
$$

Where $U(\boldsymbol{r^N})$ is the interaction potential of the N particle system. The system configuration is defined by all the positions $\boldsymbol{r^N} = \{\boldsymbol{r_1}, \boldsymbol{r_2}, \boldsymbol{r_3}, ..., \boldsymbol{r_N}\}$. $\boldsymbol{F_i}(t)$ is the force exerted on the particle i by the $(N-1)$ other particles. This implies a law of conservation of total energy $E = K + U$, where K is the kinetic energy of the particles.

In most simulations the potential is chosen as the sum of particle pair interac-

tions:

$$U(\boldsymbol{r^N}) = \sum_i \sum_{j>i} U_{ij}(\boldsymbol{r_{ij}}) \; with \; \boldsymbol{r_{ij}} = |\boldsymbol{r_i} - \boldsymbol{r_j}| \tag{3.2}$$

This is a system of differential equations that can be numerically solved by their discretization on a time step δt. which must be small enough that forces can be considered constant in this time interval. Here, we perform an iterative calculation: we first assign each particle of the system their initials position and velocities. Then, the forces acting upon the particles are calculated and, finally, the new positions and velocities are deduced. By repeating this procedure a considerable number of times, it is possible to obtain the individual trajectories in the space of the phases (FRENKEL, D.; SMIT [39]).

We must pay attention to some variables when applying MD simulation methodology. Simulation time is usually on the nanosecond scale and at the end of the simulation we need to check whether the properties of interest have stopped drastically from varying. Simulation box size can also be a challenge depending on the property of interest (TUCKERMAN [20]).

3.2   Ergodic Hypothesis

Experimentally, the measurement of a macroscopic state variable A corresponds to the average $< A >$, of a microscopic property A, calculated over a long period of time in comparison to the scale of molecular phenomena. For example, the "measurement" of the internal energy U corresponds, in fact, to the average of the energy ϵ_i of all the microstates that follow one another during the measurement. Mathematically:

$$\langle A \rangle \; = \lim_{\tau \to \infty} \left(\frac{1}{\tau} \int_{t_0}^{t_0+\tau} A(t)dt \right) \tag{3.3}$$

The ergodicity principle applied to thermodynamic systems stipulates that the time average is equivalent to an average calculated on a set of representative microstates of the system, where the weight of each configuration m to its probability

of occurrence P_m is:

$$\bar{A} = \sum_m P_m A_m \qquad (3.4)$$

This statistical average is also called the ensemble average. A_m is the microscopic magnitude, obtained from the laws of quantum or classical mechanics, associated with A in the micro-state m.

The trajectories determined are used to evaluate the static and dynamic properties by time averages, which coincide with the statistical averages for ergodic systems. Figure 3.1 illustrates the Ergodic Hypothesis.
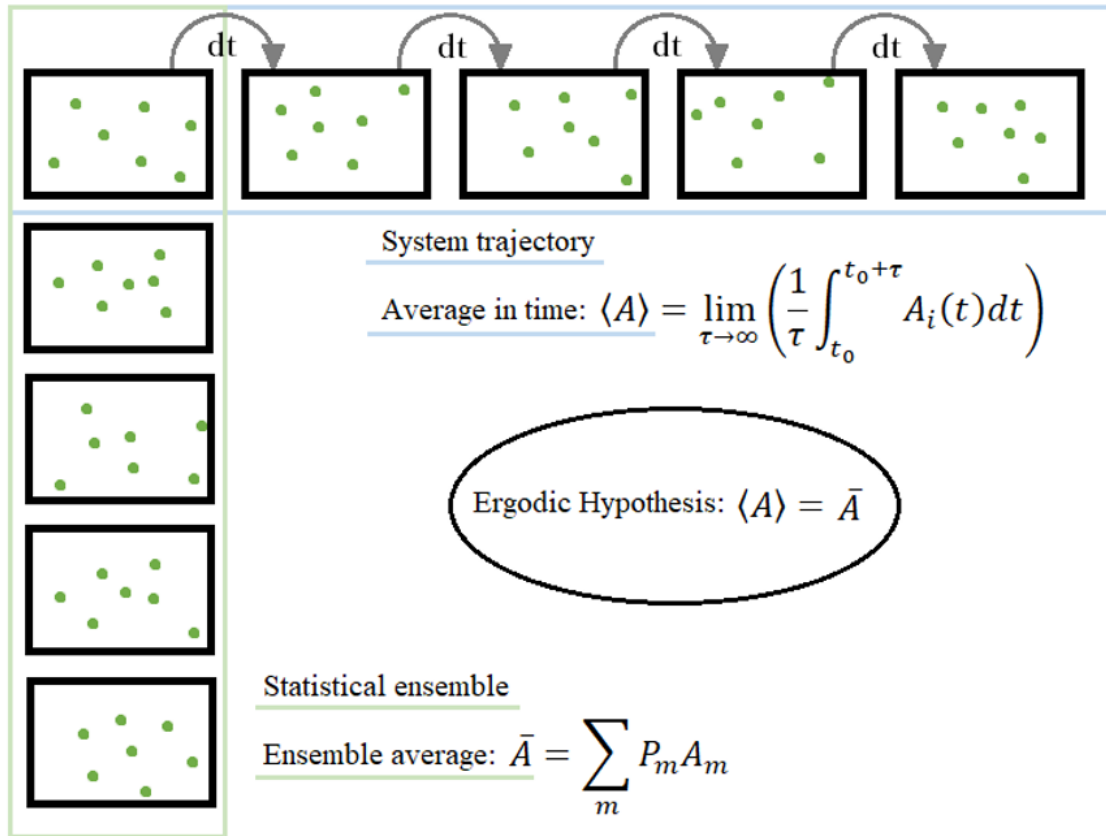

Figure 3.1: Ergodic Hypothesis Illuastration

The computational measurement of a physical quantity is obtained by the arithmetic average of the instantaneous values of this measured during the simulation. It is possible to obtain different macroscopic properties of the studied system from the collective behavior of the individual particles.

3.3 Statistical Ensemble and Integrating the Equation of Motion

3.3.1 Microcanonical

To perform calculations on any type of system the first thing to define is the control variables. In this first case, the number of particles (N), volume (V) and total energy (E) are chosen to be the control variables and they characterize the microcanonical ensemble. In order to calculate thermodynamic properties, we need to define the control variables of a system. The control variables chosen first here are the number of particles (N), volume (V), and total energy (E) (TUCKERMAN [20]).

In the classical Hamiltonian mechanics we have that:

$$\frac{d\mathcal{H}}{dt} = 0 \Rightarrow \mathcal{H}(x) = \ const. \tag{3.5}$$

And, if we have a system evolving according to Hamilton's equations:

$$\dot{p}_i = \frac{\partial \mathcal{H}}{\partial \boldsymbol{q}} \tag{3.6}$$

$$\dot{q}_i = \frac{\partial \mathcal{H}}{\partial \boldsymbol{p}} \tag{3.7}$$

Where p_i is the momentum and q_i are the generalized coordinates. As we have the Hamiltonian H(x) conservation through the equations of motion, the trajectory calculated through Equation 3.7 will naturally generate microscopic configurations belonging to a microcanonical ensemble with energy E.

The coordinate and momentum axes for each atom in a $6N$ dimensional space is defined as the phase space. The trajectory through the phase space is then the time evolution of a system in a molecular dynamics simulation. In the microcanonical ensemble, all micro states are equiprobable. The number of accessible microstates is defined by the partition function or the density of states, and is given by the

following equation for the microcanonical ensemble:

$$\Omega(N, V, E) = \frac{\epsilon_0}{h^{3N} N!} \int dp^N dr^n \delta[\mathcal{H}(p^N, r^N) - E] \tag{3.8}$$

Here, ϵ_0 is the energy unit, h is the Planck constant, and δ is the Dirac delta function. The macroscopic properties from molecular dynamics are then obtained from the relation of the microcanonical partition function to the entropy (S). Then, we obtain the famous Boltzmann formula for entropy:

$$S = k_b ln\Omega(N, V, E) \tag{3.9}$$

To determine the value of the state variables at equilibrium (T, P, μ), simply write the entropy differential:

$$dS = \frac{1}{T}dE + \frac{P}{T}dV - \frac{\mu}{T}dN \tag{3.10}$$

An integrator generates phase space vectors at discrete times that are multiples of a fundamental time discretization parameter, Δt, known as the time step. Starting with the initial condition x_0, phase space vectors $x_{n\Delta t}$ where $n = 0, ..., M$ are generated by applying the integrator or solver iteratively. The ensemble average of a property $a(x)$ and time average are related by:

$$A = \langle A \rangle = \frac{1}{M} \sum_{n=1}^{M} a(x_{n\Delta t}) \tag{3.11}$$

The Verlet algorithm (VERLET [40]) is one of many algorithms that can be used for integrating the equation of motion and it can be obtained by using the expansion of Taylor series.

In this approach, the position of a particle at a time $t + \Delta t$ is expressed in terms of its position, velocity, and acceleration at time t. Writing down the Taylor expansion for $r(t)$ around $t + \Delta t$ and dropping the error terms for readability leads to:

$$r_i(t + \Delta t) \approx r_i(t) + \Delta t \dot{r}_i(t) + \frac{1}{2}\Delta t^2 \ddot{r}_i(t) \tag{3.12}$$

Where all terms higher than second order in Δt have been dropped.

By Newton's second law we have:

$$r_i(t + \Delta t) \approx r_i(t) + \Delta t v_i(t) + \frac{\Delta t^2}{2m_i} F_i(t) \tag{3.13}$$

A velocity-independent scheme can be obtained by writing a similar expansion for $r_i\ (t - \Delta t)$:

$$r_i(t - \Delta t) \approx r_i(t) - \Delta t v_i(t) + \frac{\Delta t^2}{2m_i} F_i(t) \tag{3.14}$$

Adding and rearranging the two last equations:

$$r_i(t + \Delta t) = 2r_i(t) - r_i(t - \Delta t) + \frac{\Delta t^2}{2m_i} F_i(t) \tag{3.15}$$

This last equation is the numerical solver known as the Verlet algorithm (Verlet 1967).

Given atoms initial positions $r^{(t=0)}$ and initial velocities $v^{(t=0)}$, and chosen a time step Δt ,it is possible to use the equations above to obtain a set of coordinates and generate a trajectory of arbitrary length through time.

As we can see, the Verlet algorithm does not explicitly evolve the velocities. It is interesting to have an approach that explicitly evolves positions and velocities as a phase space is composed of both. To solve this inconvenience, in 1982, was developed a variant of the Verlet integrator that would explicitly evolve velocities (SWOPE *et al.* [41]). Considering, again, the expansion of the coordinates up to second order in Δt:

$$r_i(t + \Delta t) \approx r_i(t) + \Delta t v_i(t) + \frac{\Delta t^2}{2m_i} F_i(t) \tag{3.16}$$

It is possible to start from $r_i(t + \Delta t)$ and $v_i(t + \Delta t)$, compute $F_i(t + \Delta t)$ and evolve backwards in time to $r(t)$ according to:

$$r_i(t) = r_i(t + \Delta t) - \Delta t v_i(t + \Delta t) + \frac{\Delta t^2}{2m_i} F_i(t + \Delta t) \tag{3.17}$$

Substituting Equation 3.14 for $r_i(t + \Delta t)$ into Equation 3.15 and solving for

$v_i(t + \Delta t)$, yields:

$$v_i(t + \Delta t) = v_i(t) - \frac{\Delta t^2}{2m_i}[F_i(t) + F_i(t + \Delta t)] \tag{3.18}$$

Since we have to take the derivative of the potential energy at each time step, these recalculations of forces at each time step becomes the most computationally expensive part of the simulation.

The Verlet and velocity Verlet algorithms satisfy two properties that are crucial for the long-time stability of numerical solvers: time-reversibility and symplectic property.

3.3.2 Canonical

Depending on the desire properties, it is necessary to have other control variables. In the Canonical ensemble they are number of particles (N), volume (V) and temperature (T). However, simply integrating Hamilton's equations of motion generates a microcanonical ensemble as a consequence of the conservation of the total Hamiltonian. To generate the necessary distribution for the canonical ensemble it is necessary to mimic the effects of a thermal reservoir. It is possible to demonstrate that, by using a non-Hamiltonian set of equations of motion to model the effect of the surrounding, it is viable to prove that the equations of motion generate the desired ensemble distribution. Some authors have devoted their time solving the problems of this approach. One of them was Martyna *et al.* [42] who adopts a generalized form of the Nosé-Hoover (WILLIAM G. HOOVER [43]) approach in the form of coupled equations. The equations of motion are rewritten as Martyna *et al.*

[42]:

$$\dot{r}_i = \frac{p_i}{m_i}$$

$$\dot{p}_i = \frac{\partial V(r)}{\partial r_i} - p_i \frac{p_{\psi_1}}{Q_1}$$

$$\dot{\xi}_k = \frac{p_{\xi_1}}{Q_k} Q_k \ \ for \, k = 1, ..., M$$

$$\dot{p}_{\xi_1} = \left(\sum_{i=1}^{N} \frac{p_i^2}{m_i} - N_f k T_{ext} \right) - p_{\xi_1} \frac{p_{\xi_2}}{Q_2}$$

$$\dot{p}_{\xi_k} = \left(\frac{p_{\xi_{k-1}}^2}{Q_{k-1}} - k T_{ext} \right) - p_{\xi_k} \frac{p_{\xi_{k+1}}}{Q_{k+1}} \ \ for \ k = 2, ..., M - 1$$

$$\dot{p}_{\xi_M} = \frac{p_{\xi_{M-1}}^2}{Q_{M-1}} - k T_{ext}$$

(3.19)

There are M thermostats $\dot{\xi}_k$, with masses Q_k, and momenta p_{ξ_k}. Here, N is the Number of particles, N_f is the number of degrees of freedom (equal dN, where d is the system dimension, if there are no constrains). These equations can be shown to have the phase space distribution:

$$f \ \alpha \ exp \left\{ -\frac{1}{k_b T} \left[V(r) + \sum_{i=1}^{N} \frac{p_i^2}{2m_i} + \sum_{k=1}^{N} \frac{p_{\xi_k}^2}{2Q_k} \right] \right\}$$

(3.20)

and the conserved quantity:

$$\mathcal{H}' = V(r) + \sum_{i=1}^{N} \frac{p_i^2}{2m_i} + \sum_{k=1}^{N} \frac{p_{\xi_k}^2}{2Q_k} + \phi(r,h) + N_f k T_{ext} \xi_1 + \sum_{k=2}^{M} k T_{ext} \xi_k$$

(3.21)

where ϕ is the potential. There are still other ensembles that are defined according to the macroscopic properties of interest. Like the isothermal-isobaric ensemble

that keeps the number of particles, the pressure and the temperature as control variables. The chemical potential, volume and temperature are controlled in the grand-canonical ensemble and for the isoenthalpic-isobaric ensemble we have the constant number of particles, pressure and enthalpy. Depending on the properties to be calculated one ensemble is usually preferable to another. Just as we need to choose the ensemble, we also need to choose the integration algorithm specific to the resolution of each equation of motion.

3.4 Initial Conditions

As mentioned, to start the simulation it is necessary to define a set of initial coordinates for each atom that will be part of the dynamics. One of the possibilities is to begin with random initial coordinates, just worrying about the minimum distance between particles in order to avoid very strong repulsive forces.

For systems that contains more complex structures such as molecular crystals or biological macromolecules, X-ray crystallography can be helpful tool to obtain initial coordinates. There are several databases that can be accessed over the internet, where it is possible to find the coordinate files of various types of solids such as the Cambridge Structure Database, the Inorganic Crystal Structure Database, or the Protein Data Bank. Similarly, there are some molecule-building programs that have databases that can be accessed, such as Avogadro software distributed for free on the Internet (HANWELL *et al.* [44]). Once initial coordinates are specified, it remains to set the initial velocities.

This can be generated in several different ways. It is possible to generate an ensemble of velocities using a random number generator with the specified seed at the specified temperature. The ensemble of generated velocities can be a uniform distribution from some minimum to maximum value, scaled to produce the requested temperature. Or it can be a gaussian distribution with a mean of 0.0 and a sigma scaled to produce the requested temperature. It is also possible to set the velocities of all atoms in a group to the specified values, amongst other possibilities.

Among the available tools to build the simulation box generating the initial configuration is the software Playmol (ABREU [45]) that uses Packmol software for

packing [**?**]. The basic principle of packmol is to treat as an optimization problem the positioning of particles in their initial positions. This allows the packing of millions of atoms (**?**]).

3.5 Periodic Boundary Conditions and Minimum-Image Convention

In addition to the initial conditions it is necessary to choose the boundary conditions of the simulation box. By far, the most common boundary condition used for molecular dynamics is the Periodic Boundary Conditions (PBC). In this condition the simulation box is placed in the unit cell and considered to have infinitely images in space. This replication forms an infinite lattice in 3D space. This technique is largely used so surface effects don't dominate simulations results and allows the simulation of the bulk phase. This means that particles interact across the boundary, and they can exit one end of the box and re-enter the other end.

The periodic boundary condition can be applied to cubic and non-cubic boxes. In the case of this study, both montmorillonite and barite are positioned in cubic boxes, however, due to the shape of its unit cell, calcite presents a simulation box in the shape of a hexagonal prism with the angles $\alpha = \beta = 90°$ and $\gamma = 120°$ and the sides a = b ≠ c.

Theoretically, a particle inside a simulation box whose periodic boundary condition is being applied would be interacting with infinite other particles, which would cause a significant increase in computational time. To prevent this from happening we use the concept of minimal image convention so that each atom i interacts only with the closest periodic image of the other $N - 1$ particles. In addition, a spherical cutoff is applied to restrict this number of calculated interactions further. For a consistent combination of spherical cutoffs and the minimum-image convention, the cutoff radius (r_c) is at most $L/2$, where L is the dimension of the side of the box (TUCKERMAN [20]). Figure 3.2 is the representation of the periodic boundary condition. L is the dimension of the side of the box and r_c the cutoff radius.
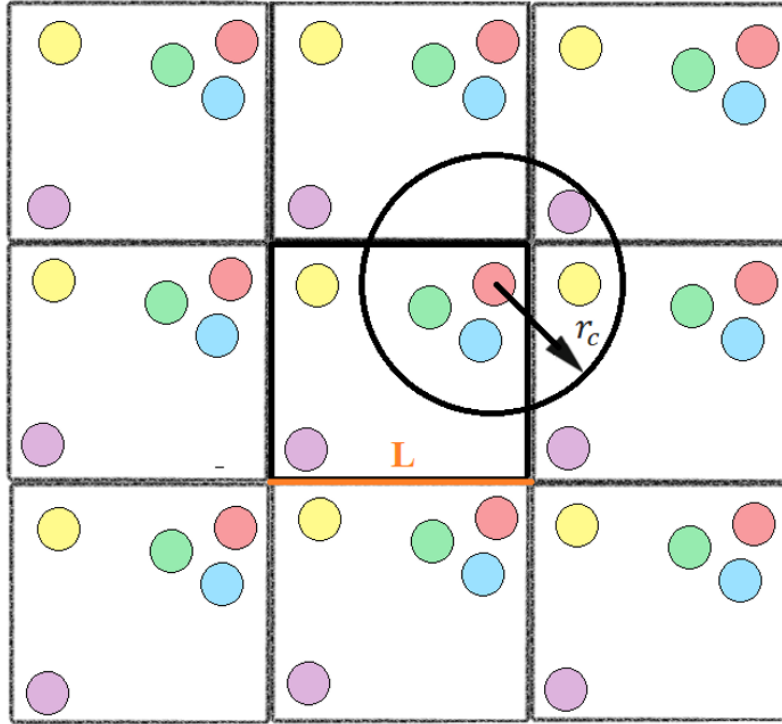
Figure 3.2: representation of the periodic boundary condition. L is the dimension of the side of the box and r_c the cutoff radius

With the application of PBC, the concept of minimum image and cut-off radius we have another problem as we have to examine each pair separation. This can be a problems depending on the number of distinct This method defines a skin (shown in Figure 3.2) around the cutoff radius with a radius r_{List}. It is build a list of all atom pairs within a neighbor cutoff distance equal to their force cutoff plus the skin distance are stored in the list. Over the course of the simulation, only pairs in the pair list interact.
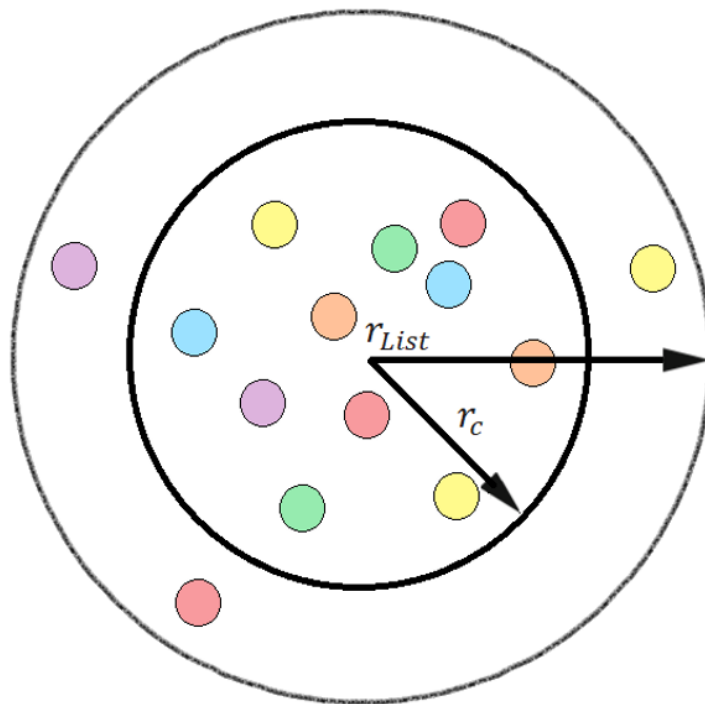
Figure 3.3: Representation the cutoff radius (r_c) and the pair list radius (r_{list})

3.6   Force fields

As previously mentioned, pair potentials (pairwise potential energy functions) are defined for atoms that are within a cutoff distance from each other and the set of active interactions typically changes over time. Therefore, we need a model for these interactions. As we need to calculate the derivative of the potential energy function $[U(r^N)]$ with respect to the coordinates in order to compute forces and update the positions during a simulation, the models chosen to represent these interactions should be simple and be able to accurately represent thermodynamic data. These models are called force fields. Force fields can describe a variety of structural characteristics such as van der Waals interactions (vdW), electrostatic interactions (eletro), cross interactions (cross), dipole interactions (pol), bond lengths (stretch), bond angles (bend) and torsion (tors) in a molecular simulation. The description is done by approximating the potential energy function, which has contributions due to intermolecular and intramolecular interactions. The intramolecular and intermolecular interactions include bond stretching, angle bending, bond torsion, van der Waals interactions, electrostatic interactions, dipole interactions and cross in-

teractions – these last two not included in this work. The final potential energy function defined by the force field is then expressed by summing all the interactions:

$$U(r^N) = U_{stretch} + U_{bend} + U_{tors} + U_{cross} + U_{vdW} + U_{eletro} + U_{pol} \qquad (3.22)$$

An illustration of some of these interactions can be seen in Figure 3.4:
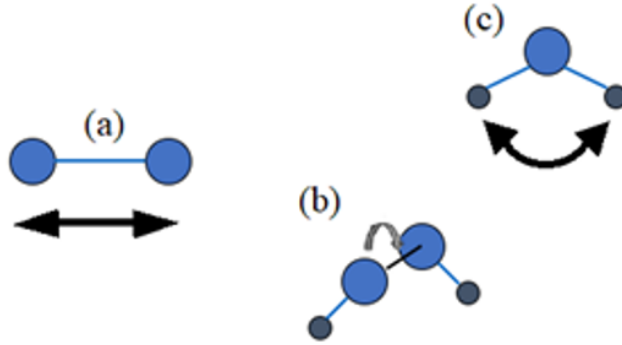

Figure 3.4: Representation of bond stretching (a), bond torsion (b) and angle bending (c).

For the intermolecular interactions or non-bonded interactions we have the most common model for pairwise dispersion−repulsion interactions called Lennard-Jones potential (LJ) (JONES [46]). The LJ potential follows the same functional form as the Mie potential (MIE [47]), but has fixed values for the exponents in the dispersion and repulsion terms. The Mie pairwise-additive potential is given by:

$$U_{Mie} = U_{rep} + U_{disp} = C\epsilon \left[\left(\frac{\sigma}{r_{ij}} \right)^{\lambda_m} - \left(\frac{\sigma}{r_{ij}} \right)^{\lambda_n} \right] \qquad (3.23)$$

Where U_{rep} is the repulsion term characterized by exponent λ_m and U_{disp} is the dispersion term characterized by exponent λ_n. For the LJ potential, they are 12 and 6 respectively. The constant C is a function of these exponents and for LJ its value is fixed at 4, ϵ is the potential well depth , σ is related to the atomic diameters and r_{ij} represents the distance between a pair of atoms i and j. The constant C is a

defined as:

$$C = \frac{\lambda_m}{\lambda_m - \lambda_n} \left(\frac{\lambda_m}{\lambda_n} \right)^{\frac{\lambda_n}{\lambda_m - \lambda_n}} \tag{3.24}$$

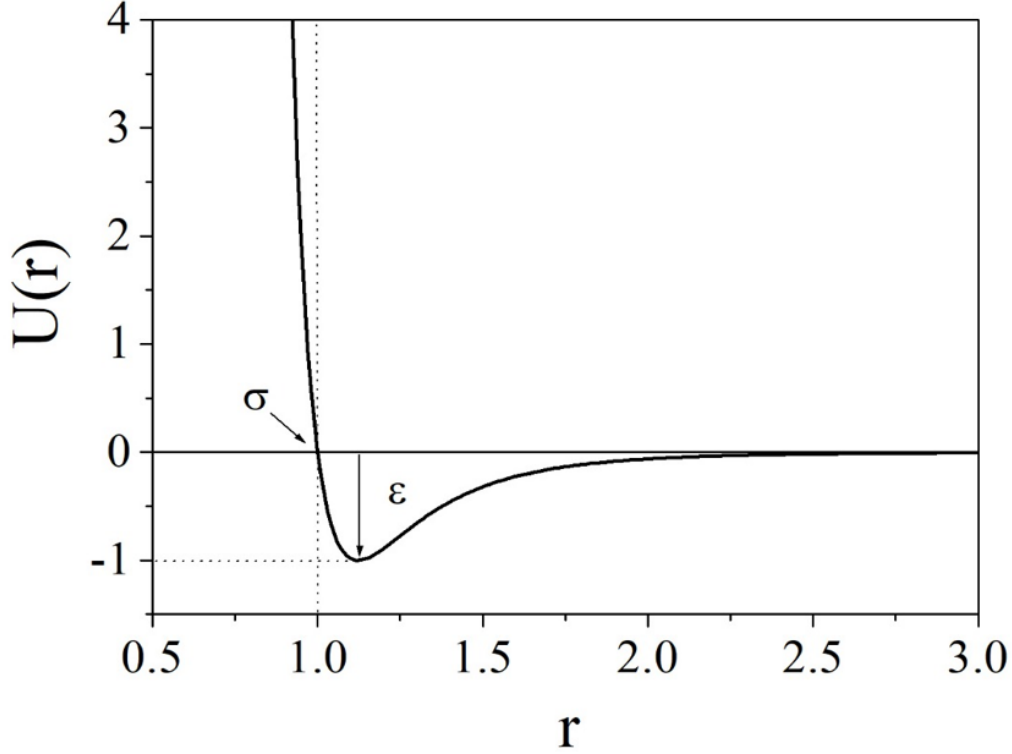The graphical representation of the Lennard-Jones potential is presented in Figure 3.5:

Figure 3.5: Lennard-Jones potential representation for $\sigma = 1$ and $\epsilon = 1$

The potential in 3.5 tends to zero and becomes negligible after a specific large value of r. In practice, this potential is truncated beyond a certain cutoff. Also, only interactions with the nearest periodic image of the cell are considered for short-range interactions. The electrostatic interactions are taken into account by using the Coulombic potential through the incorporation of partially charged sites into the potential model according to the expression:

$$U_{eletro} = \frac{q_i q_j}{4\pi \epsilon_0 r_{ij}} \tag{3.25}$$

where q_i and q_j are the partial charges of the atoms and ϵ_0 is the vacuum permittivity.

The other types of interactions, the bonded interactions, in this work are due only to bond stretching and angle bending. These contributions are usually given by the harmonic approximation:

$$U_{strech} = \frac{1}{2}k_S(r_{ij} - r_0)^2 \tag{3.26}$$

$$U_{bend} = \frac{1}{2}k_B(\theta_{ijk} - \theta_0)^2 \tag{3.27}$$

Both energy expressions increase the potential energy using force constants k_S and k_B and deviations from the equilibrium geometry (r_0 and θ_0), which is given by an approximation around the energy minimum.

Chapter 4

Methodology

One of the main tasks of this work was to build a protocol to create a simulation box that contained a solid crystal. The first solid studied was montmorillonite, whose composition is $(Na_3(Si_{31}Al)(Al_{14}Mg_2)O_{80}(OH)_{16}$ (CYGAN *et al.* [7]). Montmorillonite is a dioctahedral smectite clay with monoclinic symmetry. It is characterized by aluminum substitution for magnesium in the octahedral sheet with silicon substitutions for aluminum in the tetrahedral sheet (CYGAN *et al.* [7]). From the Ca-montmorillonite structure $(Al_2Si_4O_{12}Ca_{0.5})$ available in the Avogadro software (HANWELL *et al.* [44]), whose unit cell size is 5.18, 8.89 e 6.642 Å in directions x, y, and z, respectively – the Na-montmorillonite unit-cell used in this work was built according to the modifications represented in Figures 4.1, 4.2 and 4.3. Namely, it consists in replacing oxygen with hydroxyl (Figure 4.1), silicon by aluminum at the octahedral sheet (Figure 4.2) an and aluminum by magnesium (Figure 4.3) according to the unit cell disclosed in the work of Cygan *et al.* [7]. Care was needed to avoid overlapping atoms in the moment of replication the unit-cell as well as not leaving empty spots.
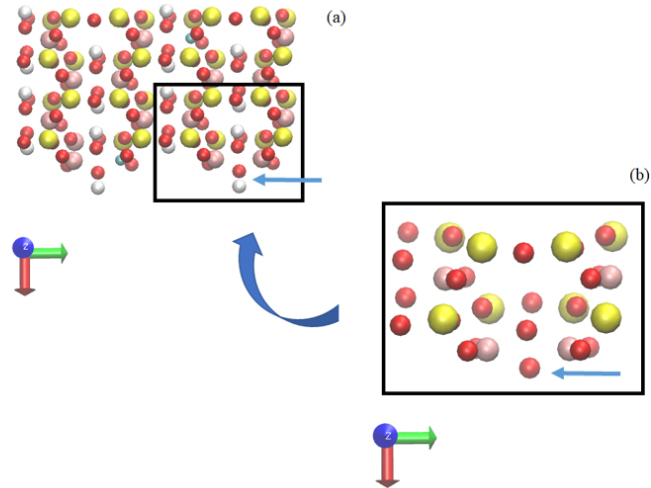
Figure 4.1: Plan Z view of the montmorillonite unit cell (a) Na-montmorillonite (b) Ca-montmorillonite. The light blue arrow indicates the replacement of an oxygen atom in (b) by a hydroxyl group in (a). (Color scheme: silicon – yellow, oxygen – red, hydrogen – white, aluminum – pink, magnesium – cyan).
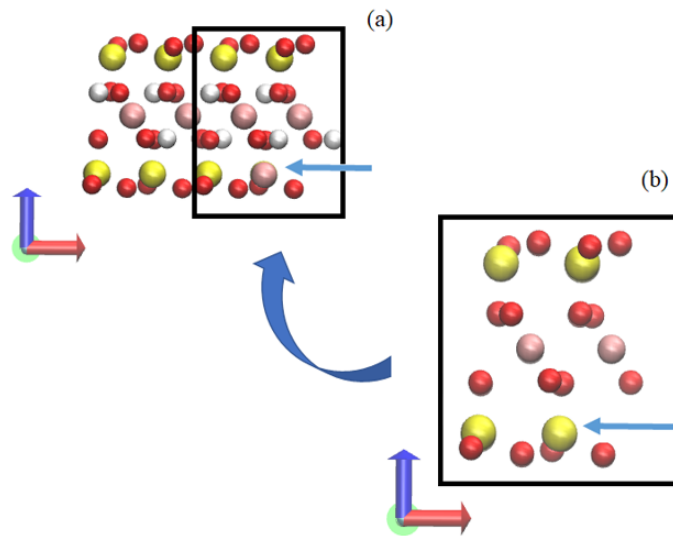

Figure 4.2: Plan -Y view of the montmorillonite unit cell (a) Na-montmorillonite (b) Ca-montmorillonite. The light blue arrow indicates the replacement of a silicon atom in (b) by an aluminum atom in (a) at the tetrahedral sheet.
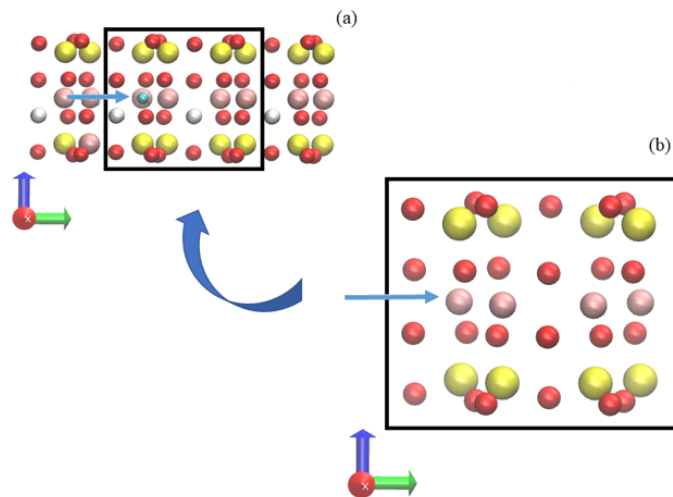
Figure 4.3: Plan X view of the montmorillonite unit cell (a) Na-montmorillonite (b) Ca-montmorillonite. The light blue arrow indicates the replacement of an aluminum atom in (b) by a magnesium atom in (a) at the octahedral sheet.

After the building of the unit-cell, it was necessary to use a replication tool to generate the clay plate. Thus, a code for the building the simulation box using Playmol (ABREU [45]) was written and used to replicate the unit-cell in the x and y dimensions respecting the Na-montmorillonite unit-cell size which is 10.382, 17.961 and 6.642 Å respectively as shown in the demonstrate the building of the plate in the y direction.
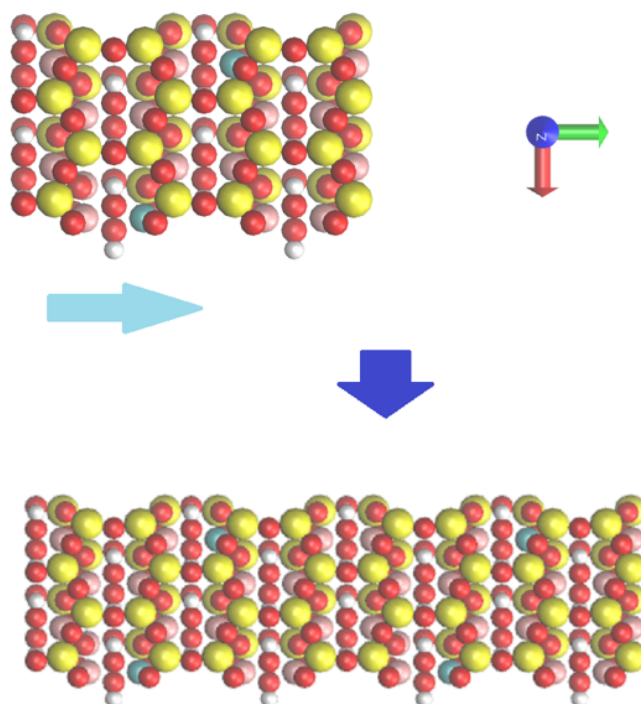
Figure 4.4: Protocol demonstration of the building of the plate in y direction. The light blue arrow indicates the replication direction and the dark blue arrow shows two units cells

The next step was to build a simulation box with the solid plates and the fluid. The initial configuration is assembled as follows: a single montmorillonite crystal is placed at the bottom of the box, and the rest of the box is filled with the fluid molecules. The second slit-like pore structure is actually formed by the images resulting from the periodic boundary condition applied to the z direction, which is the direction perpendicular to the crystal surface.

Initial tests were performed to ensure solid integrity during the NVT simulation. The cutoff radius was chosen to be 15 Å. Figure 4.5 shows a snapshot of the beginning and on the end of an montmorillonite, test where one can see that the solid retained its shape throughout the simulation.
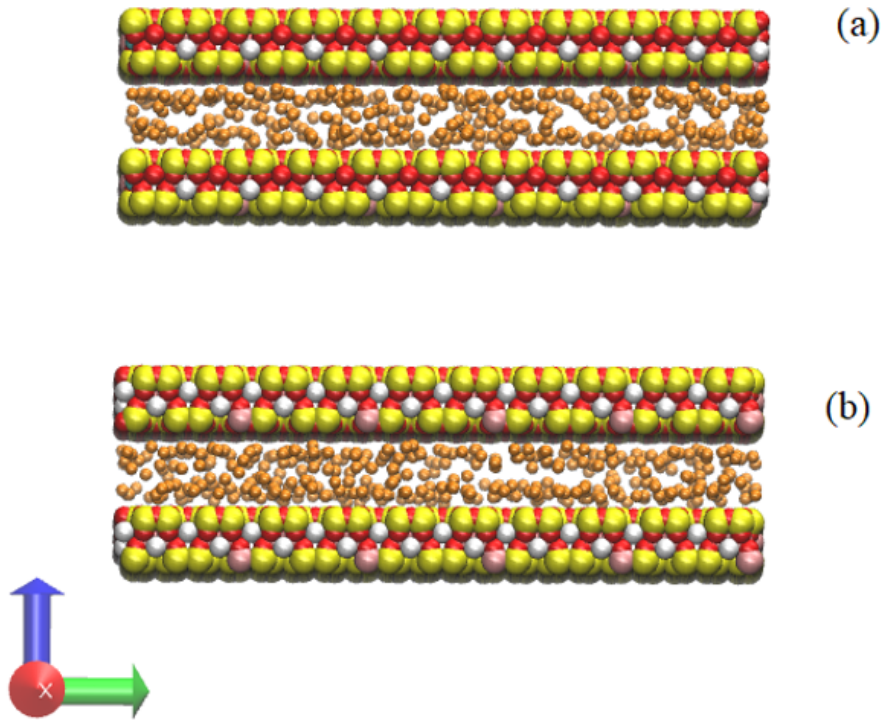
Figure 4.5: Snapshot of the beginning (a) and end (b) of simulation of an montmorillonite nanopore filled with a mixture of methane (cyan) and nitrogen (orange).

A pore containing a large amount gas is a an idealization of what might occur during the injection of mixtures of CO_2 + CH_4, and N_2 + CH_4 streams inside the pores. We selected a range of densities following the work of Santos *et al.* [13]. For pure substances the density inside the pore was approximately 166 kg/m^3 and for the mixture twice that, approximately 332.0 kg/m^3. The confined fluids are studied in terms of local density as a function of the z coordinate because of the anisotropic behavior of the pressure tensor in the pore. Molecular dynamics (MD) simulations of slit-shaped nanopores of montmorillonite (montmorillonite), barite, and calcite containing mixtures of CO_2 + CH_4, and N_2 + CH_4 were carried out to analyze the effects of the solid wall on the adsorption of each compound.

All of the MD simulations were performed using the Large-scale Atomic/Molecular Massively Parallel Simulator (LAMMPS) package (STEVE PLIMTON [48]). The NVT ensemble was considered so as to keep the pore volume constant. The atoms of solid the matrix were kept immobile. A time step of 1.0 fs was used, and the equations of motion for a system under the influence of a Nosé-Hoover chain thermostat (WILLIAM G. HOOVER [43], MARTYNA *et al.*

[49]) were integrated with the reversible algorithm described by Martyna [42]. Coulombic and van der Waals contributions represent the nonbonded energies (Equations3.23 and 3.25) , and the stretch and bend terms represent the bonded energies – harmonic potential for both angle and bond (Equations 3.26 and 3.27) were used as in Cygan *et al.*'s work [4].

Standard Lorentz−Bertholet mixing rules are used to evaluate heteroatomic interactions. The unlike size parameters are obtained using the arithmetic-mean combining rule for the molecular diameter, that is:

$$\sigma_{ij} = \frac{\sigma_{ii} + \sigma_{jj}}{2} \tag{4.1}$$

The parameters for unlike-pair energy interactions are calculated using the geometric-mean combining rule:

$$\epsilon_{ij} = \sqrt{\epsilon_{ii}\epsilon_{jj}} \tag{4.2}$$

Methane was represented as a single-site molecule and TraPPE (MARTIN and SIEPMANN [5]) was the force-field used for it. For carbon dioxide, the non-bonded interaction parameters were taken from Cygan's force field [4] and CO_2 was modeled as a fully flexible three-sit, while nitrogen was represented with a rigid three-site model taken from Vujić's work [6]. The force fields used for montmorillonite, barite, and calcite were, respectively, CLAYFF (CYGAN *et al.* [7]), MSXX (JANG *et al.* [8]), and the model proposed by Xiao [9]. The force field parameters for both solids and fluids are summarized in Tables 4.1, 4.2 and 4.3. Where σ is related to the atomic diameters, ϵ is the potential well depth, q is the pseudo-atom charge, k_{bond} is the bond constant, r_o is the equilibrium bond distance, k_{angle} is the angle constant, θ_o is the equilibrium value of the angle.

Table 4.1: Force-field parameters for methane, carbon dioxide and nitrogen. (CYGAN *et al.* [4], MARTIN and SIEPMANN [5], VUJIĆ and LYUBARTSEV [6])

Pseudo-atom	σ Å	ϵ kJ/mol	q e	k_{bond} kJ/molÅ^2	r_o Å	k_{angle} kJ/mol rad^2	θ o
CH$_4$	3.730	1.231	0.0	–	–	–	–
C (in CO$_2$)	2.800	0.234	+0.651	8443	1.162	451.9	180°
O (in CO$_2$)	3.028	0.668	−0.326				
N (in N$_2$)	3.320	0.303	−0.482	–	0.549	–	180°
M (N$_2$)	0.000	0.000	+0.964				

Table 4.2: Force-field parameters for montmorillonite (CYGAN *et al.* [7])

Pseudo-atom	σ Å	ϵ kJ/mol	q e
Si in MMT	3.706	7.70x10-6	+2.100
Al in MMT	4.794	5.56x10-4	+1.575
Mg in MMT	5.909	3.38x10-6	+1.360
O in MMT	3.553	0.650	−1.030 / −1.081
H in MMT	0.000	0.000	0.000
Na in MMT	2.580	0.418	+1.000

Table 4.3: Force-field parameters for barite, and calcite (JANG *et al.* [8], XIAO *et al.* [9])

Pseudo-atom	σ A	ϵ kJ/mol	q e
Ca in CaCO$_3$	2.370	2.000	1.668
C in CaCO$_3$	2.604	3.690	0.999
O in CaCO$_3$	3.091	0.582	−0.889
Ba in BaSO$_3$	6.942	5.02x10^{-3}	2.000
S in BaSO$_3$	4.000	1.439	1.544
O in BaSO$_3$	3.405	0.407	−0.885

The molecular configurations used to initialize the simulations were generated

using the Playmol package (ABREU [45]) and initial velocities were assigned using a Gaussian random number generator with standard deviation compatible with the specified temperature, according the Maxwell-Boltzmann distribution. A particle-particle-particle mesh (PPPM) solver (HOCKNEY and EASTWOOD [50]) was used with a desired relative error in forces of $1 \times 10-4$ to calculate the long-range Coulombic interactions. Standard long-range corrections to the energy was also included, and conventional periodic boundary conditions over the x, y, and z directions were applied. Thus, the slit-shaped crystal nanopores have infinite surface area. Figures 4.6, 4.7 and 4.8 illustrates the unit cells of the three solids. The x × y dimensions of the simulation box were set equal to 62.293 × 89.806 Å^2 for montmorillonite and the Miller index for the crystal was 001, 28.61 × 44.395 Å^2 for barite with the Miller index also 001, and 29.95 × 43.23 Å^2 for calcite with the Miller index 110. Pore widths were specified by following the studies by Cygan *et al.* [4] and Santos *et al.* [13] and specified as 13.0 Å for montmorillonite, and 30.0 Å for calcite and barite. This range of widths was defined considering experimentally measured pore size distributions of shale and tight hydrocarbon reservoirs, molecular dynamics and Monte Carlo simulations and the fact that confinement effects are negligible in wider pores (BOŢAN *et al.* [51], ZHANG *et al.* [52]). In Figures 4.9, 4.10 and 4.11 we present the plates formed from the unit cells
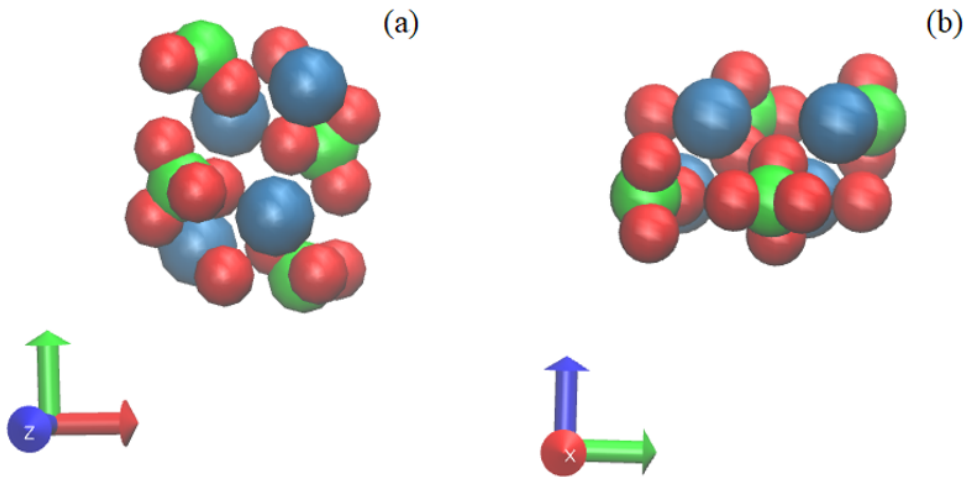

Figure 4.6: Barite unit cell, plan Z view (a), plan X view (b) (color scheme: barium – dark blue, sulfur – green, oxygen - red).
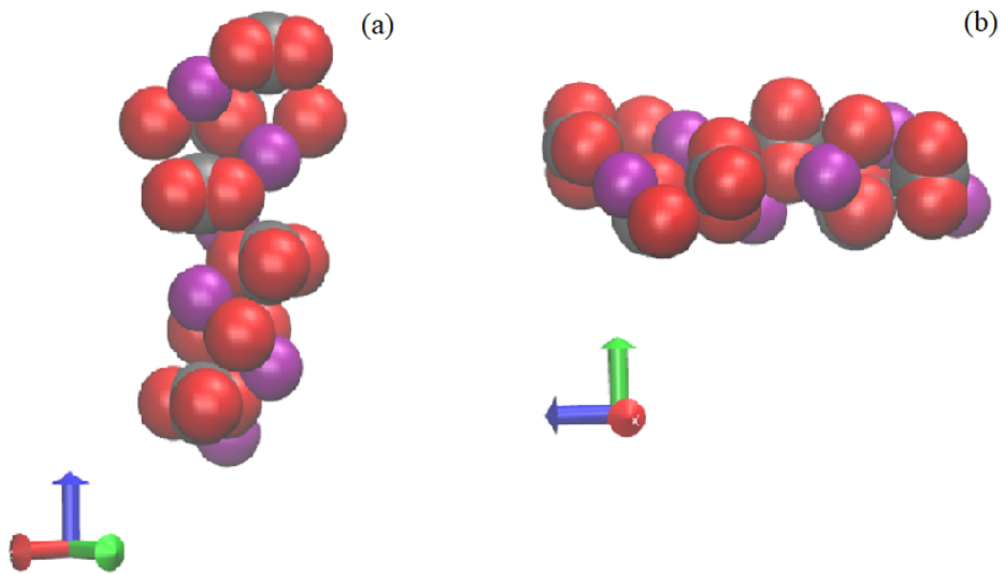
Figure 4.7: Calcite unit cell, plan XY view (a), plan X view (b) (color scheme: calcium – purple, carbon – gray, oxygen – red).
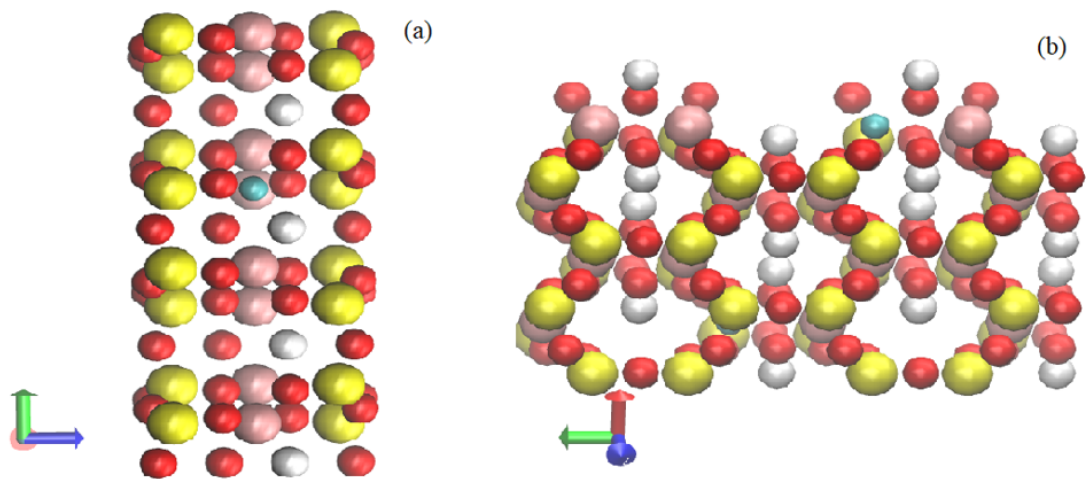

Figure 4.8: Montmorillonite unit cell, plan -X view (a), plan Z view (b) (color scheme: silicon – yellow, oxygen – red, hydrogen – white, aluminum – pink, magnesium – cyan).
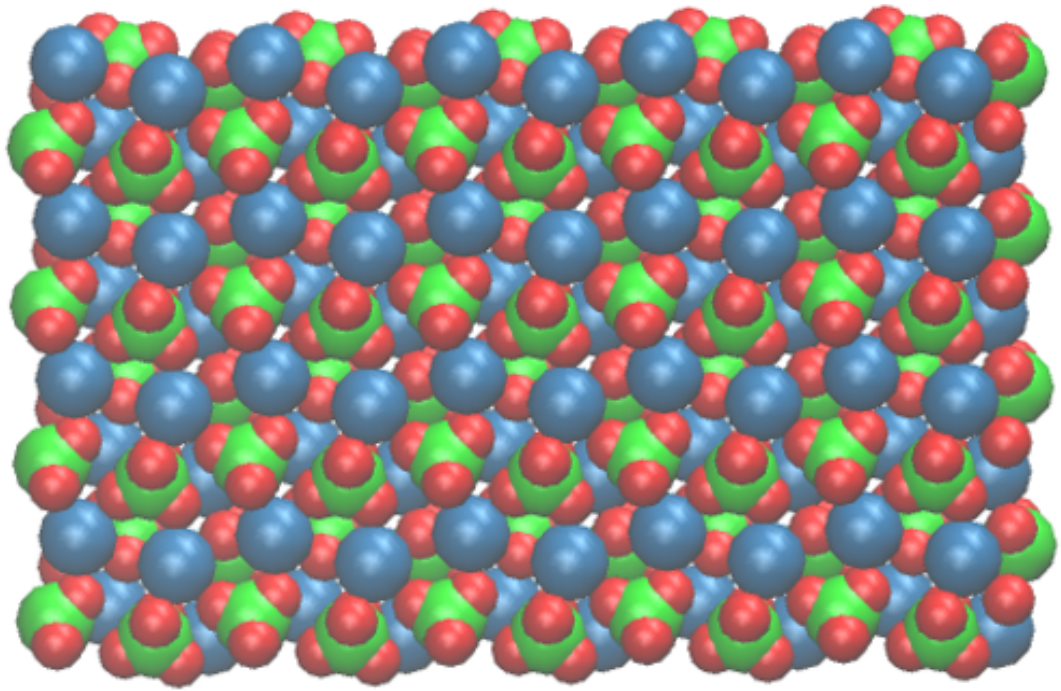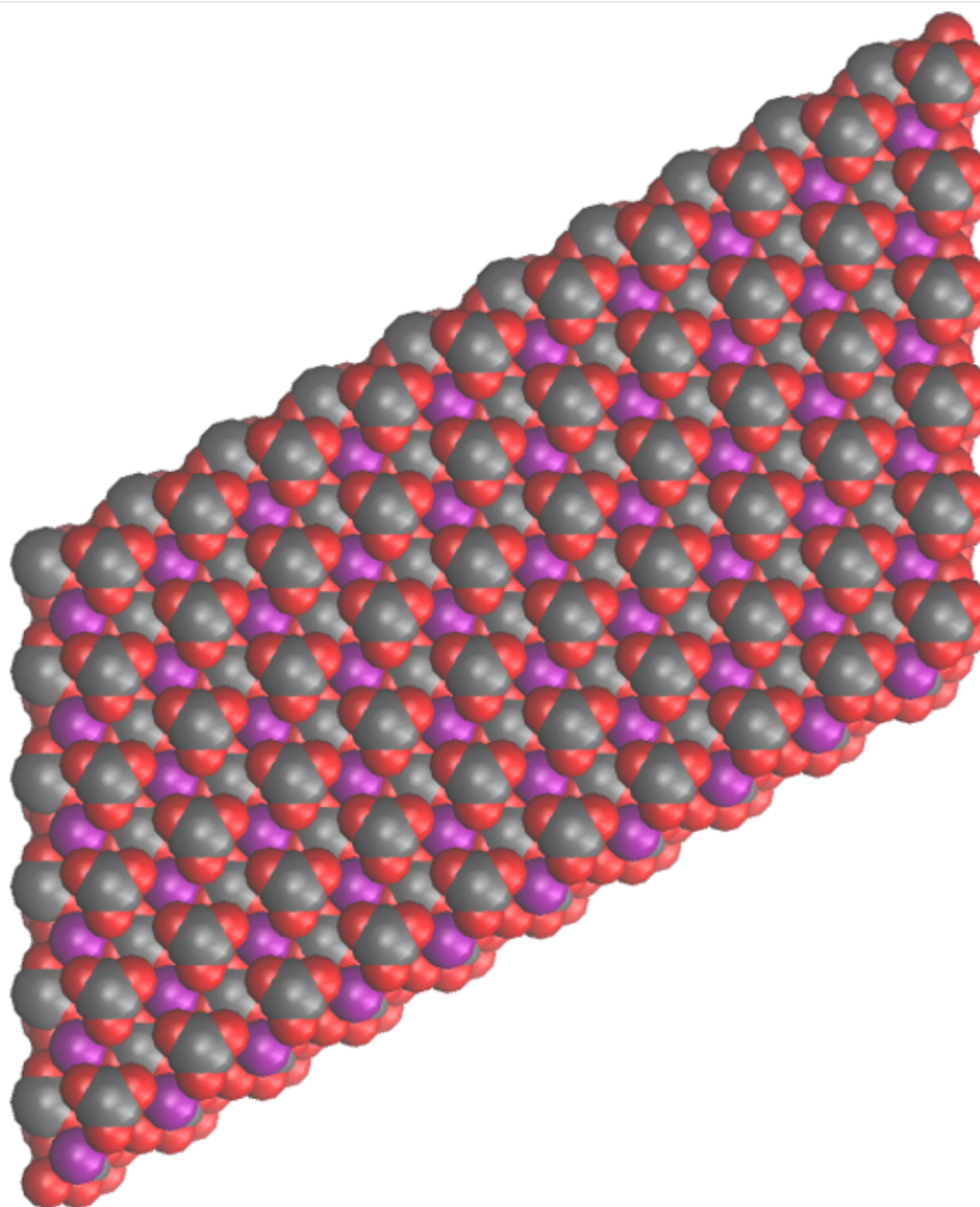
Figure 4.9: Top view of the barite plate.

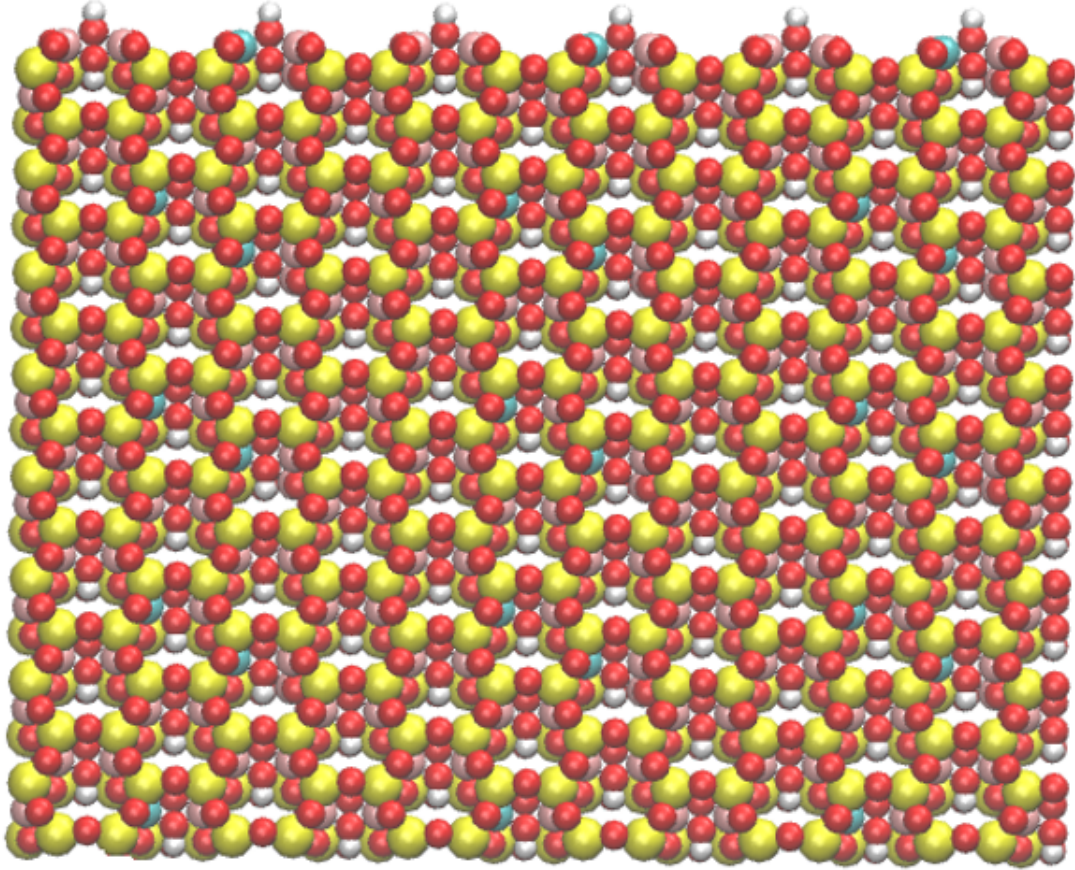Figure 4.10: Top view of the calcite plate.

Figure 4.11: Top view of the montmorillonite plate.

Given an initial configuration of the fluid molecules, during equilibration, asymmetries between the density profiles in the fluid−solid interfaces at the bottom and at the top of the simulation box are expected to arise. We then, perform an annealing process in order to facilitate the equilibration (LEONI and FRANZESE [53], SALGADO-BLANCO *et al.* [54]). Initial tests were performed to analyze the results with different equilibration times and after considerations we decided to start by simulating the system at the temperature of 500 K for 1 ns, then we slowly lower the temperature to 300 K with this process lasting 4 ns. At last, we simulate the system for 2 ns at 300 K. After this equilibration process, the ensemble average was studied. The production time was 4 ns, during which the positions were recorded every 0.1 ps so that the density profile could be calculated by splitting the simulation box into parallel slabs and calculating the density average in each one. The simulation boxes were divided into 66, 50, and 71 slabs for montmorillonite, calcite and barite respectively after a brief study that analyzed the best discratization .

Chapter 5

Results and Discussion

The main goal of this work was to study mixtures of CO_2 + CH_4 and N_2 + CH_4 inside three different types of nanopores and observe the impact of one component on the adsorption of the other one on the pore wall. We also intended to analyze whether depending on the solid, the adsorption profile of each substance changes. With this in mind, changes in the behavior of the components and the distribution along the pores were monitored after inserting the components in equal mass, so that the integral of the density profile in the pore is the same for both, as the following equation,

$$\int_0^{L/2} \rho(z) A dz = \frac{m}{2} \tag{5.1}$$

where $L/2$ is the distance up to the middle of the box, $\rho(z)$ is the local density, A is the cross-sectional area of the coordinates $x - y$, m is the total mass of the component. The simulation boxes right after their assemblies are shown in the Figures 4.10 and 4.11.
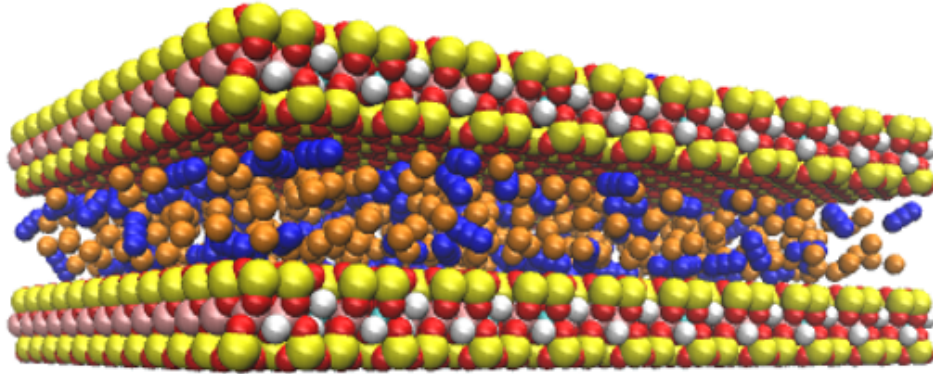
Figure 5.1: Nanopore of montmorillonite filled with methane (orange) and carbon dioxide (blue).
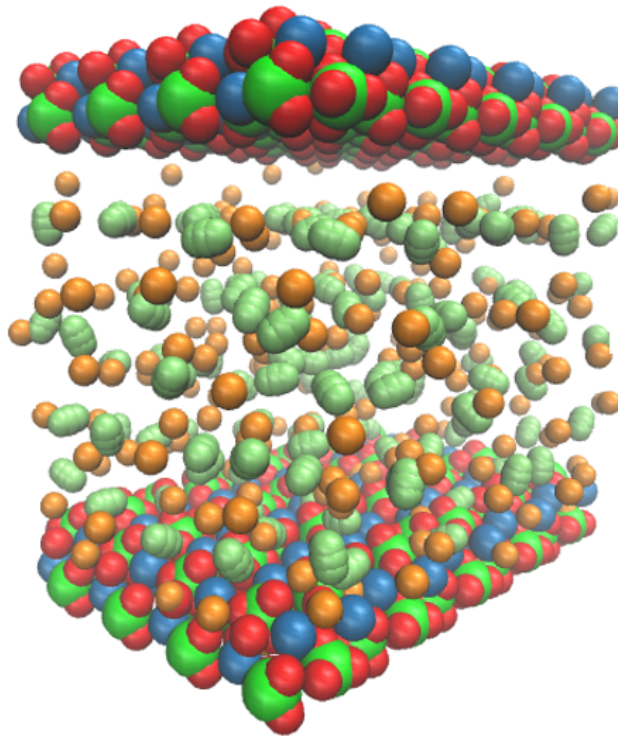

Figure 5.2: Nanopore of barite filled with methane (orange) and nitrogen (light green).

The calcite study was initially done to validate the methodology based on the work of Santos *et al.* [13]. The difference is that, here, we apply a flexible force field for CO_2 as suggested in the work of Cygan *et al.* [4] later in the work of Aimoli, *et al.* [55] for obtaining results with higher accuracy. A flexible force field for CH_4

was also tested, but the obtained results (not shown) were not significantly different from those with the simpler force field. As the use of a flexible model demands smaller time steps due to the motion of light hydrogen atoms, leading to a larger computational effort, a united-atoms force field was chosen for this component.

Figure 5.3 shows the density profiles of pure CH_4, CO_2, and N_2 up to the middle of the slit pore of barite. When in contact with this solid, all substances have a preference to be concentrated closer to the pore wall. Carbon dioxide has higher preference, followed by nitrogen and methane.
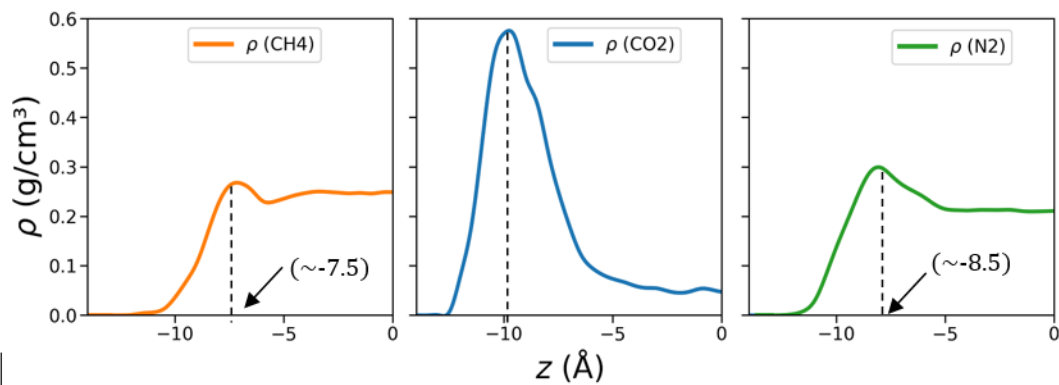

Figure 5.3: Density profile of pure substances (CH_4 – orange, CO_2 – blue, N_2 – green) inside barite slit-pore.

As can be seen, the above graph suggests that nitrogen and methane are repulsed to the wall as it is located at -14.5 Å. Carbon dioxide can get closer with a peak at -10 Å while nitrogen and methane peak at approximately -8.5 and -7.5 Årespectively. Both methane and nitrogen are smaller molecules than carbon dioxide, if only the entropic effects were considered, it was expected that smaller molecules could pack better. However, the effects of attraction and repulsion are computed through both the Lennard-Jones equation and the Coulomb equation. Both CH_4 and N_2 appear to be repulsed by the wall. After some distance they have a smaller packing than carbon dioxide due to the computed forces.

For calcite, whose obtained density profiles are shown in Figure 5.4, pure substances exhibit a slightly different behavior. CO_2 has a preference for the wall, expressed as a peak of 1.8 g/cm3. Nitrogen follows in second place, and methane shows a similar behavior in third place. Carbon dioxide exhibits a large quadrupole moment, thus adsorbents with polar surfaces, have a strong interaction with CO_2.
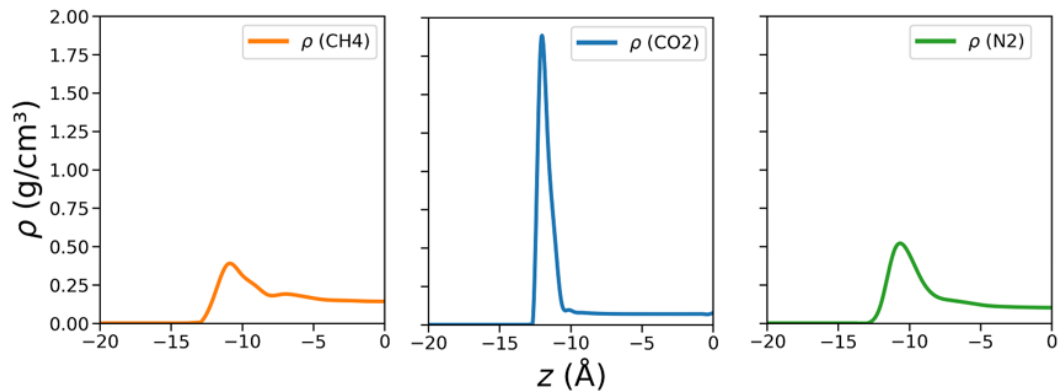
This doesn't happen with CH_4 and N_2.

Figure 5.4: Density profile inside Calcite slit-pore of pure components (CH_4 – orange, CO_2 – blue, N_2 – green).

For montmorillonite, presented in Figure 5.5, methane, carbon dioxide and nitrogen exhibit similar behavior, reaching a density of approximately 0.6 g/cm^3 closer to the wall. The graph suggests that fluid / wall interactions for the three components were felt similarly. There is no preference of any component over another even though the three components have different molecular properties.
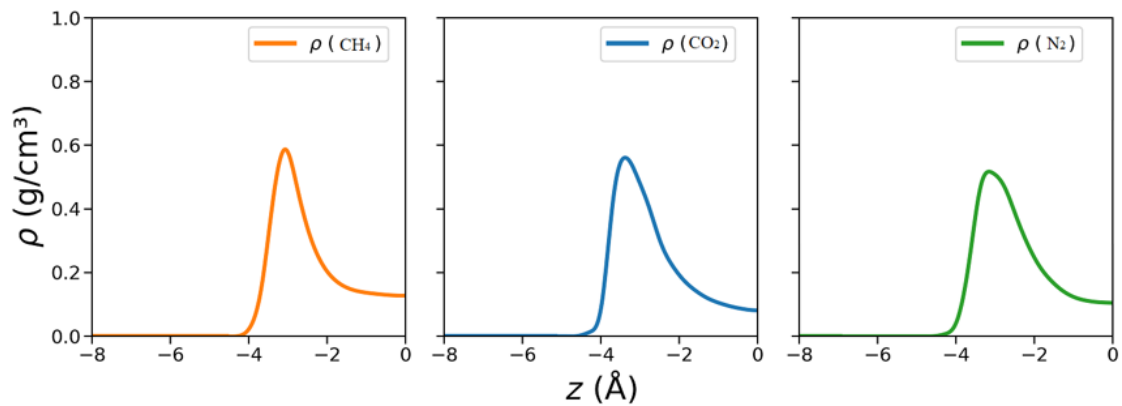

Figure 5.5: Density profile inside montmorillonite slit-pore of pure components (CH_4 – orange, CO_2 – blue, N_2 – green).

In the case of the mixtures of CO_2 + CH_4 and N_2 + ceCH4 in slit pores of barite, it can be seen in Figure 5.6 that, when compared to Figure 5.5, the CO_2 behavior remained the same.
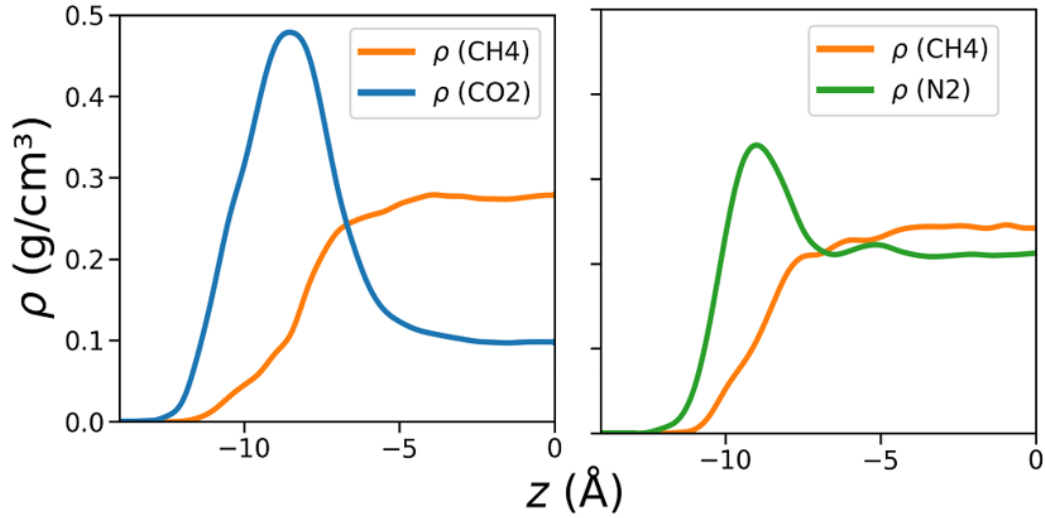
Figure 5.6: Density profiles of the mixtures of CO_2 + CH_4 (right) and CH_4 + N_2 (left) inside a slit pore of barite.

However, CH_4 did not exhibit any preference to be concentrated close to the wall. Similarly, this also happened with CH4 in the N_2 + CH_4 mixture. Figures 5.7, 5.8 and 5.9 show the barite pore snapshot filled only with methane, calcite pore filled with methane and CO_2, and barite pore filled with N_2 and CH_4 and their density profiles inside the pore. It is worth remembering that the graphs are averaged over a 4 ns after the equilibrium in the simulation is reached. Thus, a single snapshot does not represent the average behavior in the simulation. An example of is Figure 5.7, where the graph shows the highest density closest to the wall, but this cannot be seen in the simulation snapshot. It is possible to observe that the displacement of the molecules is visible which justifies the behavior of the graphs for the case of Figures 5.8 and 5.9.

Figure 5.7: Density profiles (a) and final snapshot (b) from a simulation with barite nanopore filled with methane (orange).

Figure 5.8: Density profiles (a) and final snapshot (b) from a simulation with barite nanopore filled with methane (orange) and nitrogen (green).
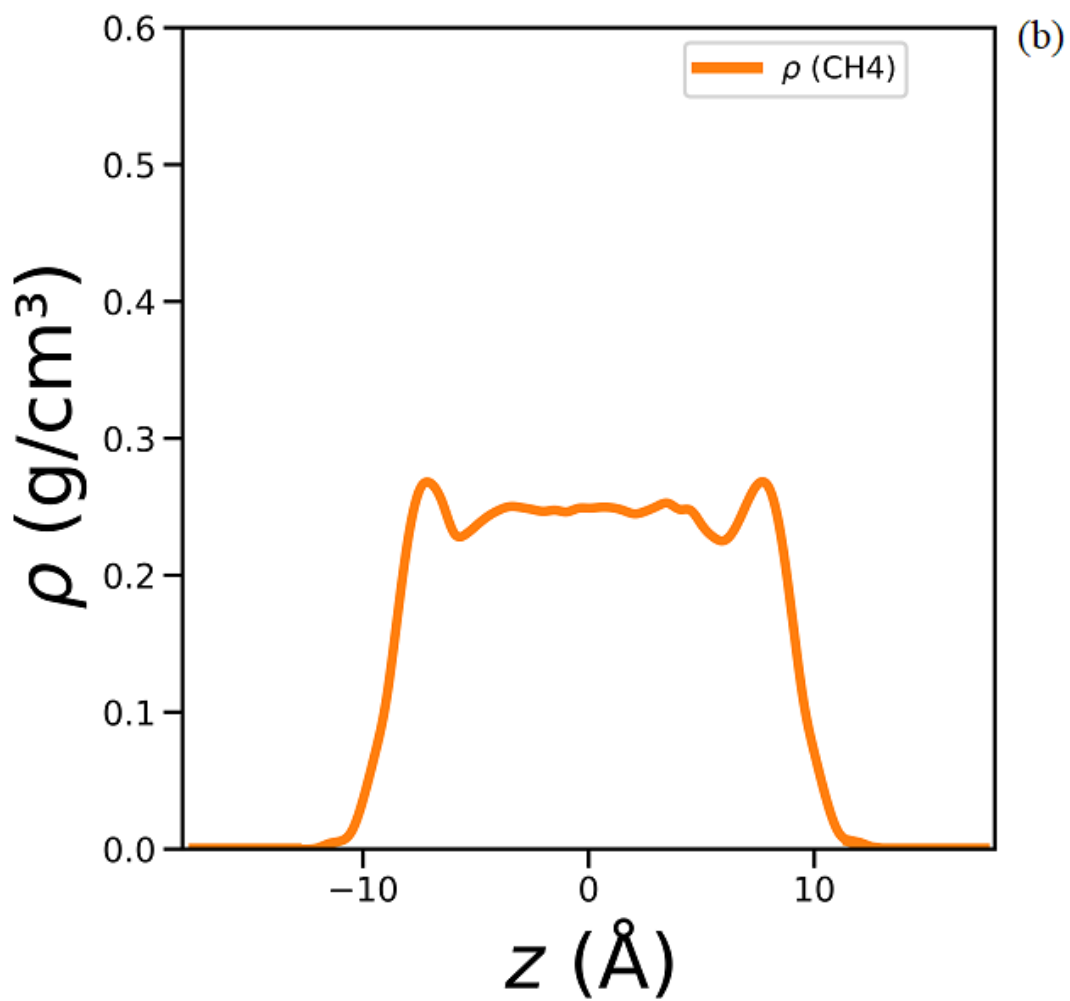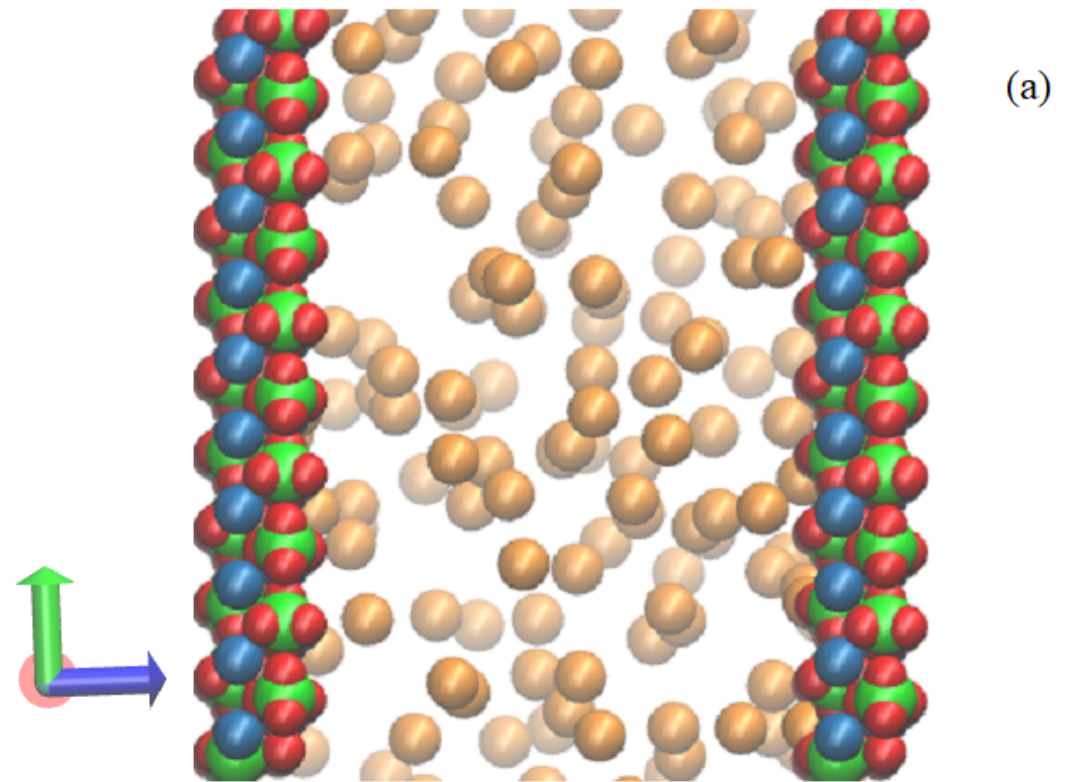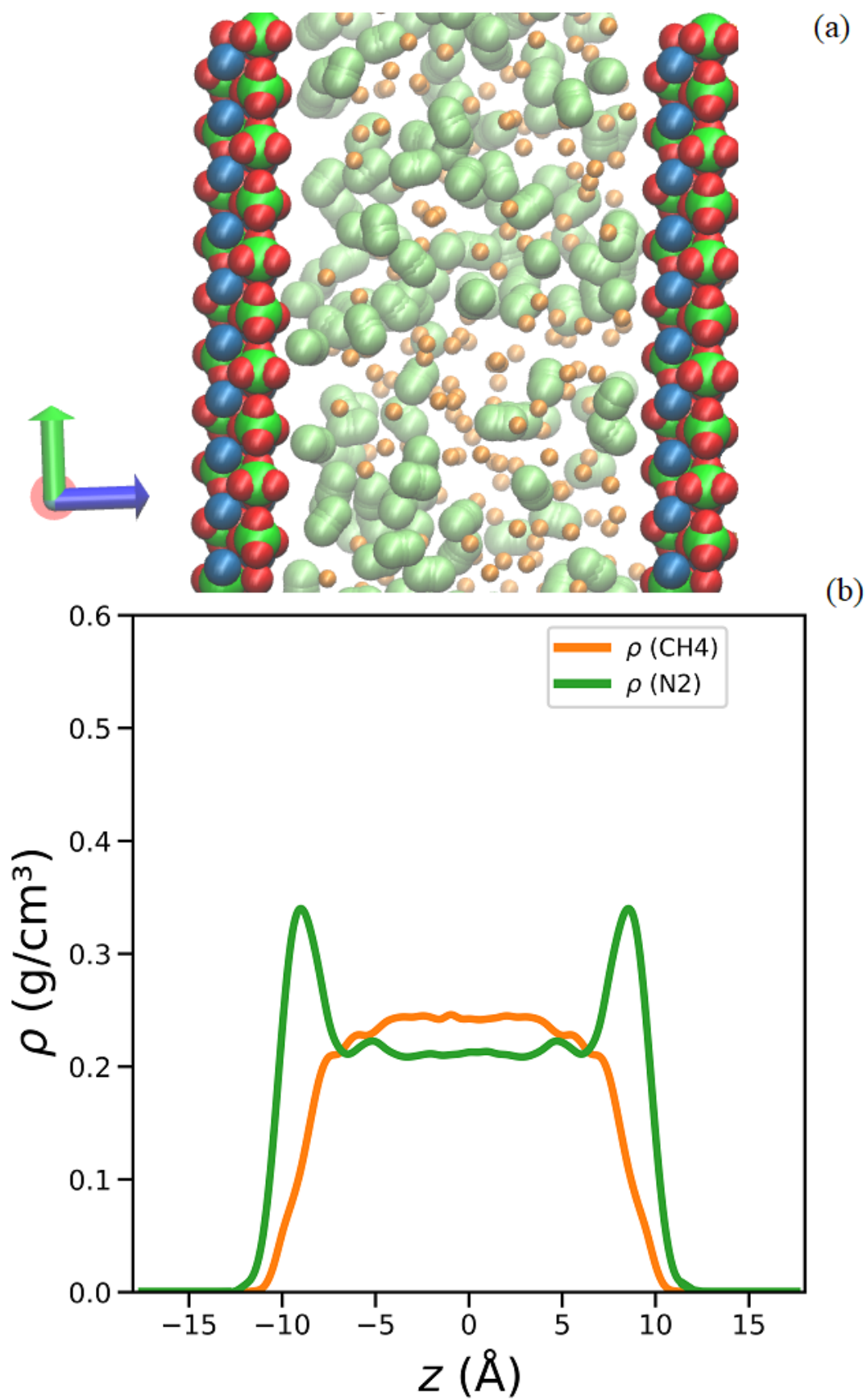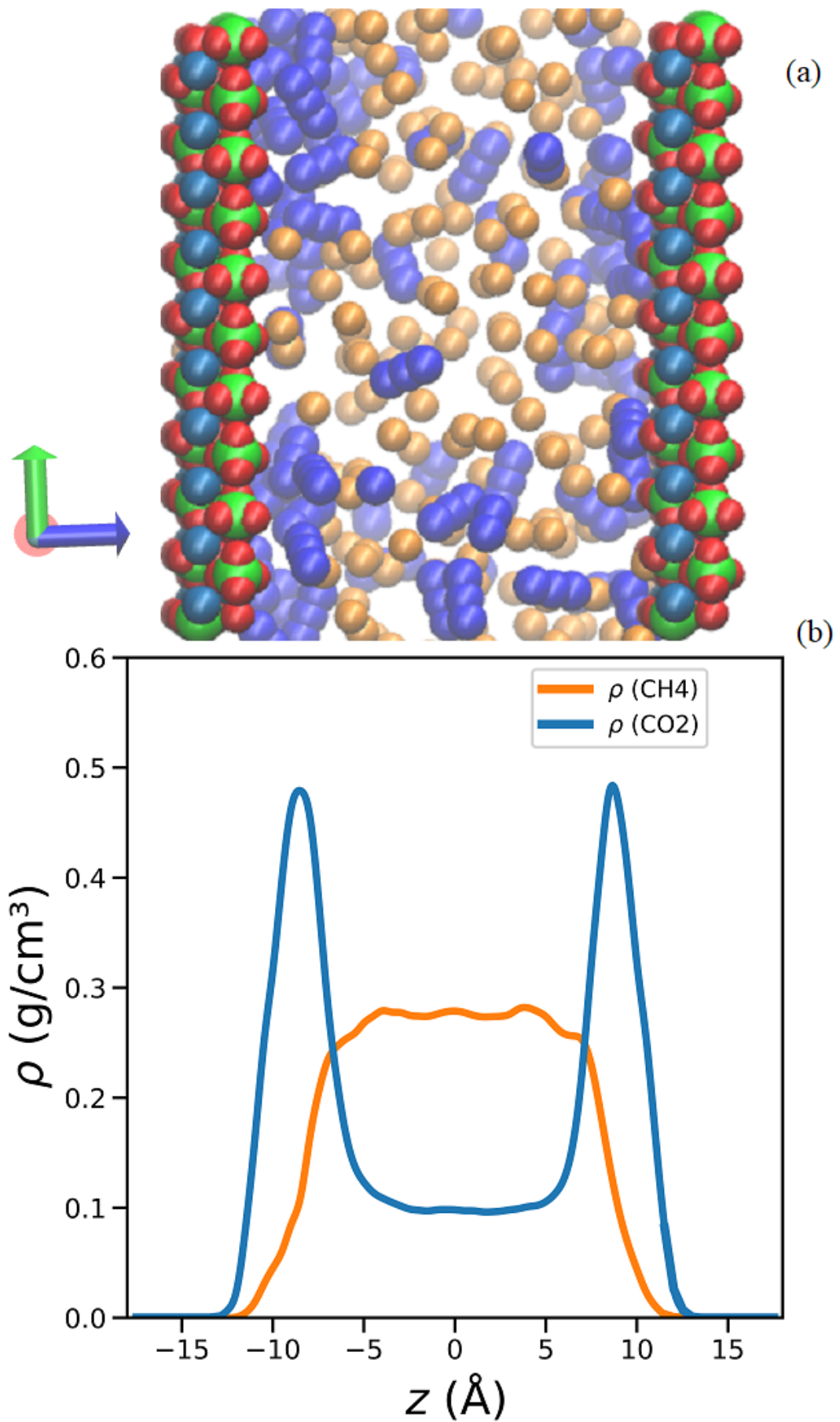
Figure 5.9: Density profiles (a) and final snapshot (b) from a simulation with barite nanopore filled with methane (orange) and carbon dioxide (blue).

In addition, the width of the region with the highest density of N_2 in the mixture decreased in comparison to the pure substance case. It can be observed that there is a much sharper separation of the CO_2 + CH_4 mixture than of the N_2 + CH_4 one, which was already expected. The high affinity of the barite surface's for CO_2, when compared to methane, is attributed to the stronger polarity of CO_2. Methane and nitrogen are known to be difficult to separate from each other because of their similar polarities, both being considered non polar substances. In any case, the density profiles of N_2 + CH_4 in the barite pore are quite interesting because this was the only solid in which such mixture exhibited some degree of separation. CO_2 + CH_4 mixture is the one that undergoes the best degree of separation in the calcite pore, as shown in Figure 5.10, corroborating the results in the work of Santos *et al.* [13]. Figures 5.11 and 5.12 show snapshots from the end of the simulation of the calcite pore filled only with methane and of the calcite pore filled with methane and carbon dioxide. Their corresponding density profiles inside the pore are also shown. Although it cannot be assumed that the behavior of the snapshot is always similar to the graphic, there are times that is possible to observe that the displacement of the molecules is visible and corroborates the behavior illustrated in the graphs.
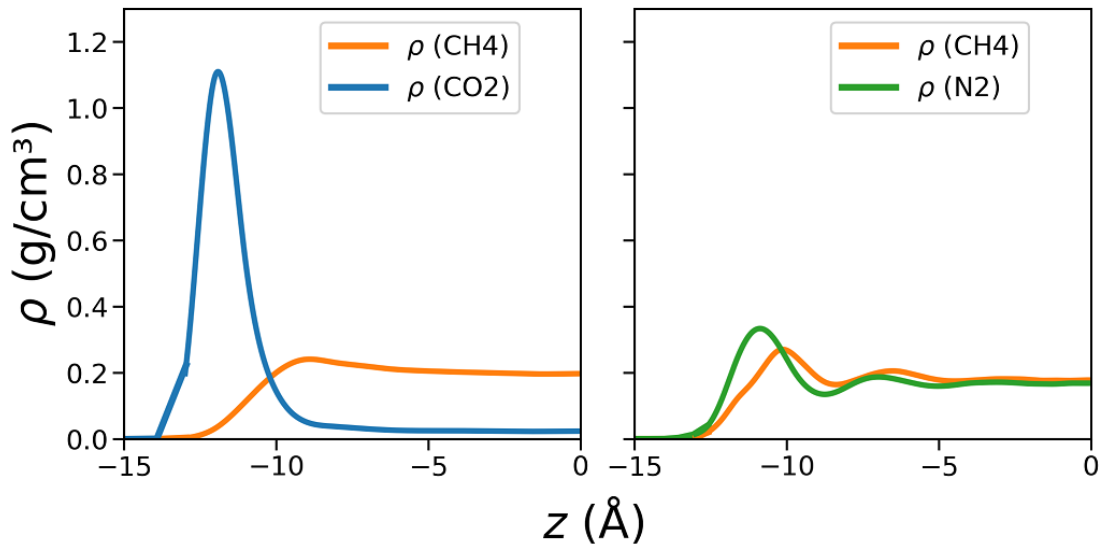
Figure 5.10: Density profiles of the mixtures of CO_2 + CH_4 (right) and CH_4 + N_2 (left) within a calcite slit-pore.
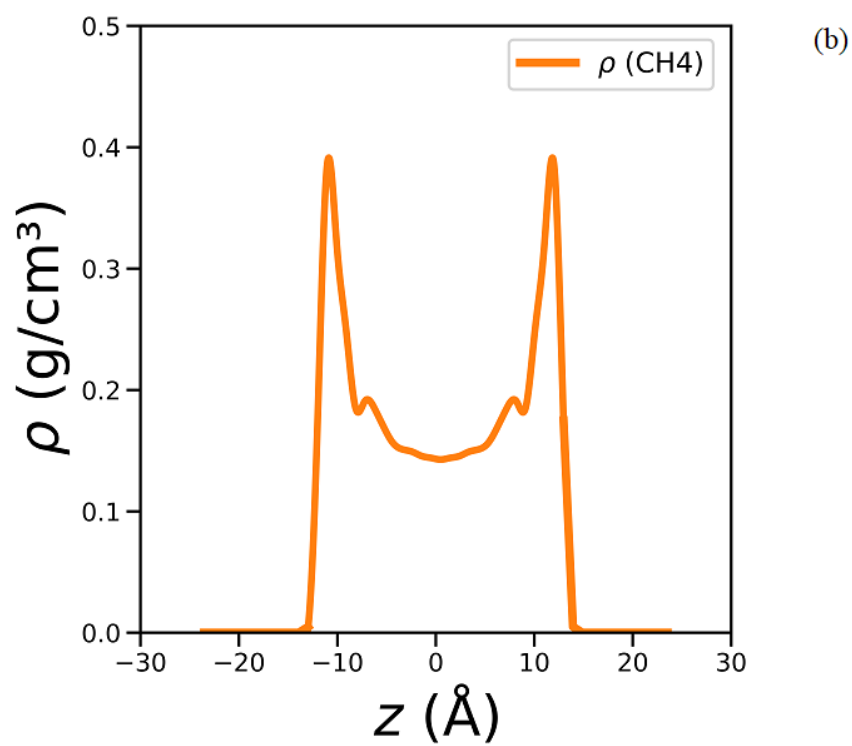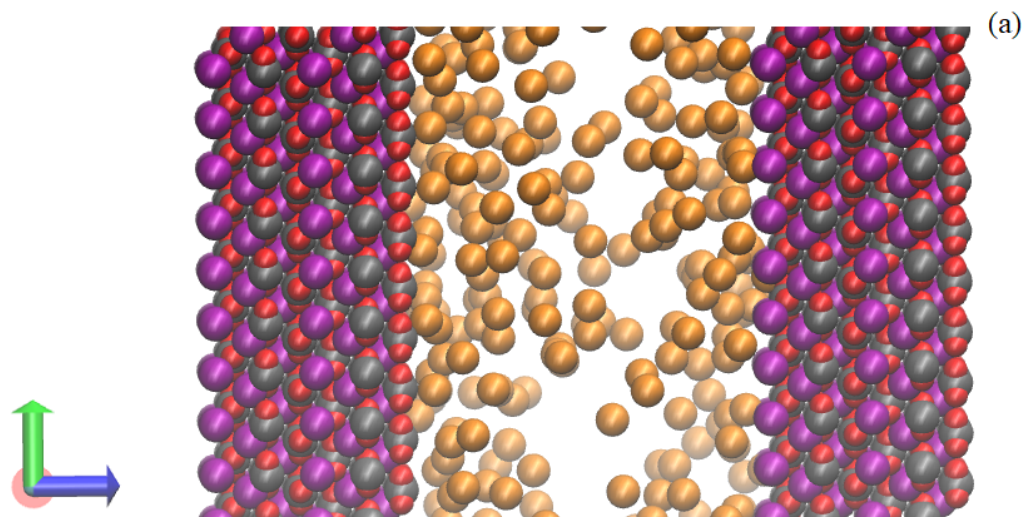
Figure 5.11: Snapshot from the end of the simulation (a) and density profiles (b) with calcite nanopore of filled with methane (orange).
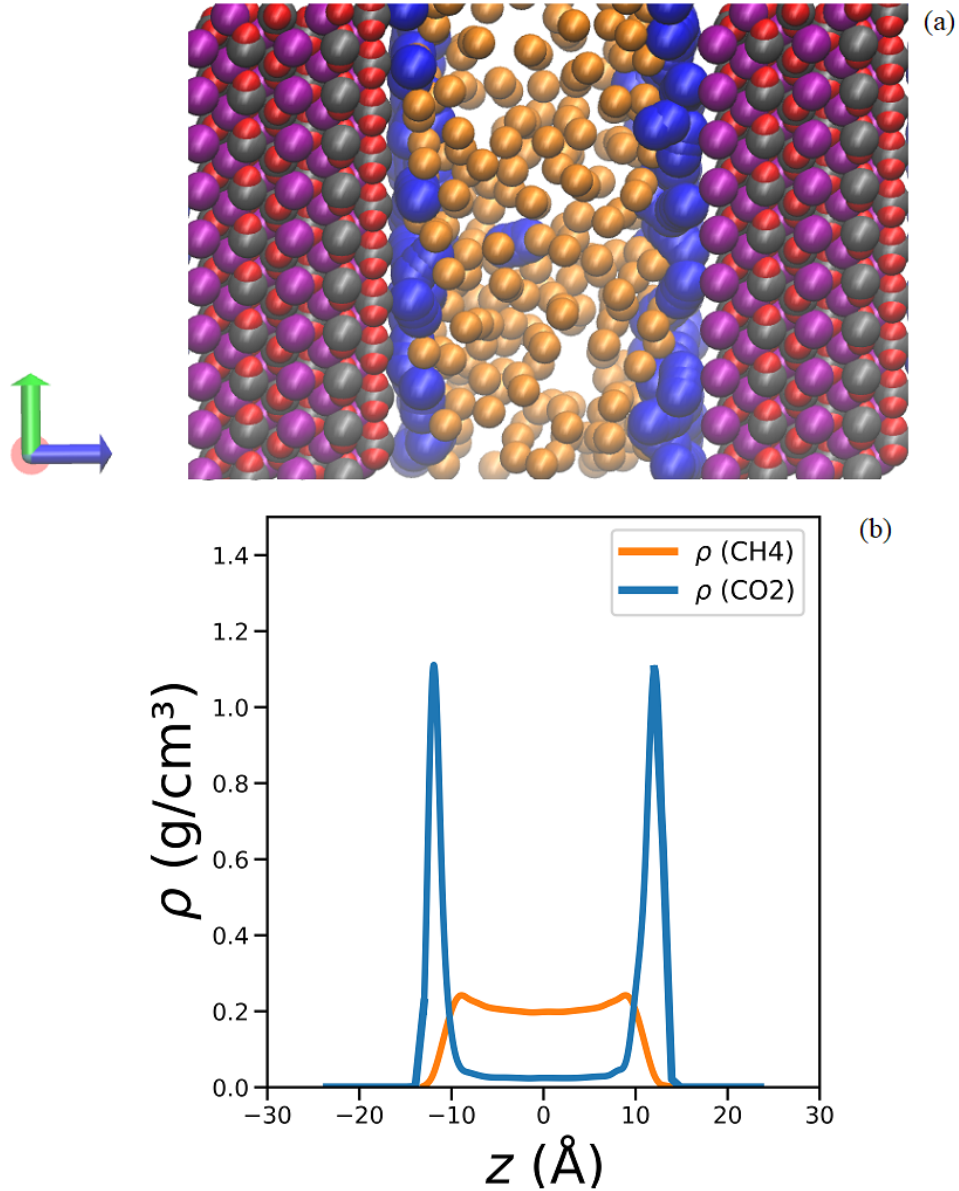
Figure 5.12: Snapshot from the end the simulation (a) and density profiles (b) with calcite nanopore of filled with methane (orange) and carbon dioxide (blue).

The high preference of CO_2 for calcite causes methane to be displaced towards the center of the pore, promoting the greatest separation among all of the studied cases. This is not observed for the mixture of methane with nitrogen. The affinity for the wall is higher for nitrogen than for methane, but the density difference closer to the wall is, in fact, small. It is observed that the greatest change in the calcite pore occurs in the behavior of methane, whose density near the wall reaches 0.4 g/cm^3 when pure and drops to 0.3 g/cm^3 when in mixture. Inside the pore

of montmorillonite, CO_2 occupies the first position in preference for the wall, but methane is not very far behind. Right after the initial layer of CO_2, there is also a layer of CH_4 near the wall of the pore, as one case observe in Figure 5.13.

Figure 5.13: Density profiles of the mixtures of CO_2 + CH_4 (right) and CH_4 + N_2 (left) within a montmorillonite slit-pore.

With the mixture of N_2 + CH_4, the two components have very similar behaviors as both have a small affinity for the wall. Since montmorillonite has a narrow pore, it is observed in the right hand side of Figure 31 that both mixture components form peaks of density located at the center of the pore. This phenomenon also happens for methane in the mixture with carbon dioxide.

As previously described, tests were done by doubling the pore size and maintaining the number of molecules, decreasing the overall density, as shown in Figure 5.14. The behavior turned out to be quite intuitive, with a broader distribution throughout the pore and a wall adsorption proportional to the decrease in the overall density. For montmorillonite, as shown in the Figure 5.15, when the pore size doubled, the peak in the center was no longer observed. This is explained by the facts that the pore of the montmorillonite is 60% smaller than the pore of barite and calcite and molecules have a tendency to form a layer layer in contact with the pore wall. Another interesting fact, specifically in this case, was that CO_2 was able to move from the center of the pore (Figure 5.13) closer to the wall.
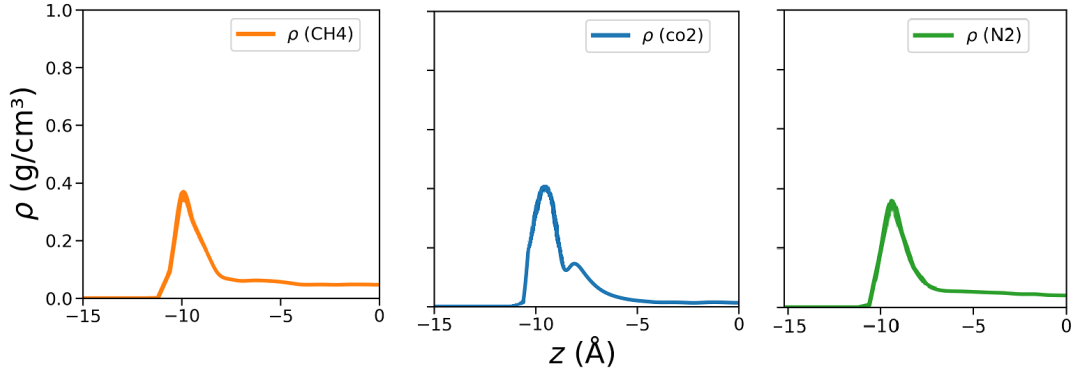
Figure 5.14: Density profile inside a double sized montmorillonite slit-pore of pure components (CH4 – orange, CO_2 – blue, N_2 – green).
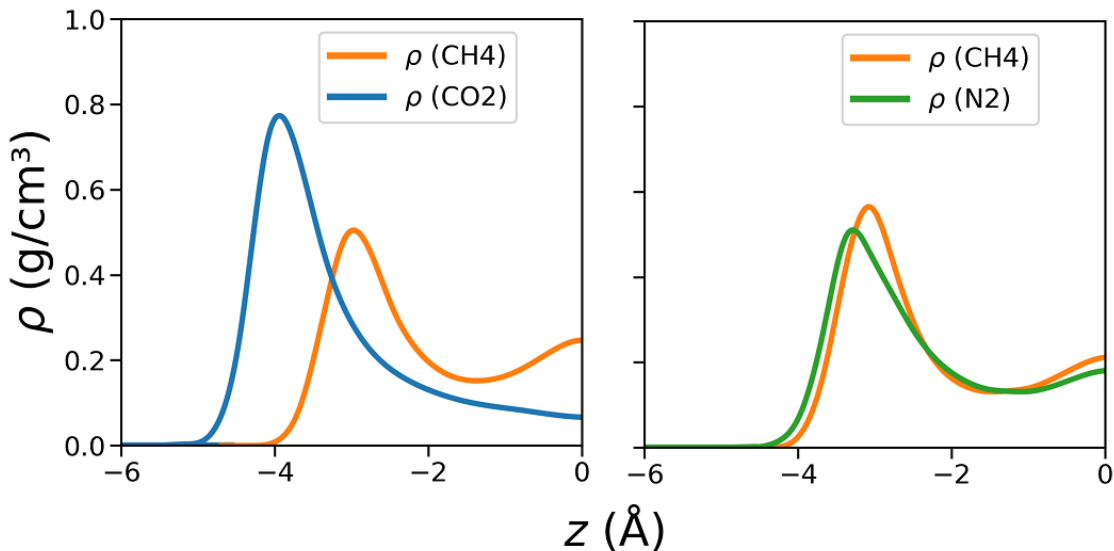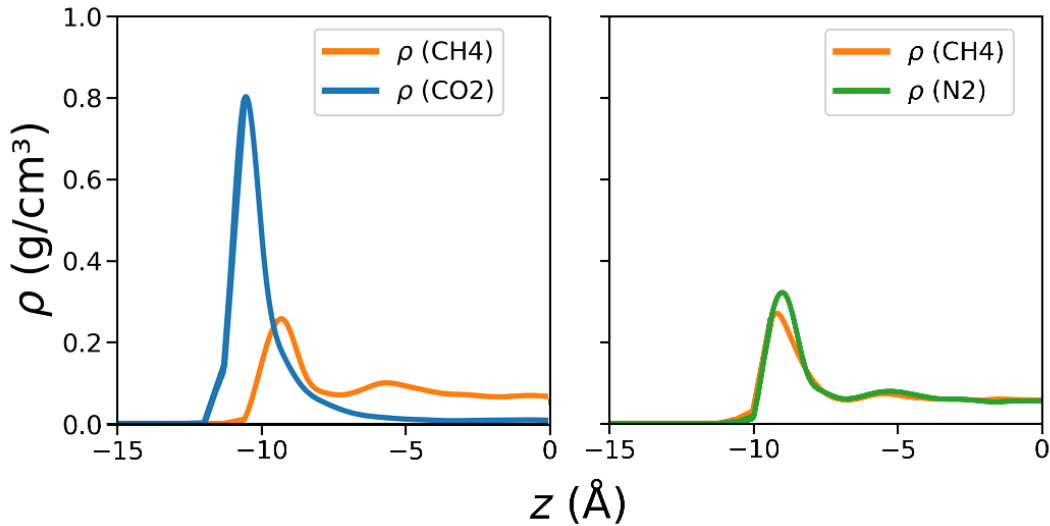

Figure 5.15: Density profiles of the mixtures of CO_2 + CH_4 (right) and CH_4 + N_2 (left) within a montmorillonite slit-pore.

To evaluate the effect of temperature in these systems, some tests were carried out at different temperatures, namely 300 K and 258 K. In general, the preference of CO_2 and N_2 for the wall increases in most solids with the reduction in temperature. The selectivity decreases with the temperature, which can be due to the fact that the entropic effects are dominant at higher temperatures, while, the adsorbate–adsorbent interactions are more significant at lower temperatures. As a result of reduction in temperature, energetic effects become more important relative to entropic effects, leading to an increase of molecules concentration at the pore wall. However, as shown in Figures 5.16, 5.17 and 5.18, the actual change is not

particularly significant.
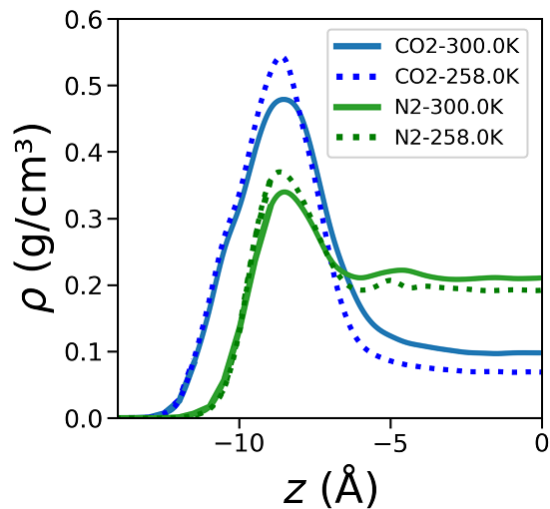
Figure 5.16: Density profiles of the CO_2 (blue) in mixtures of CO_2 + CH_4 and N_2 (green) in CH_4 + N_2 mixtures within a barite slit-pore varying the temperature.
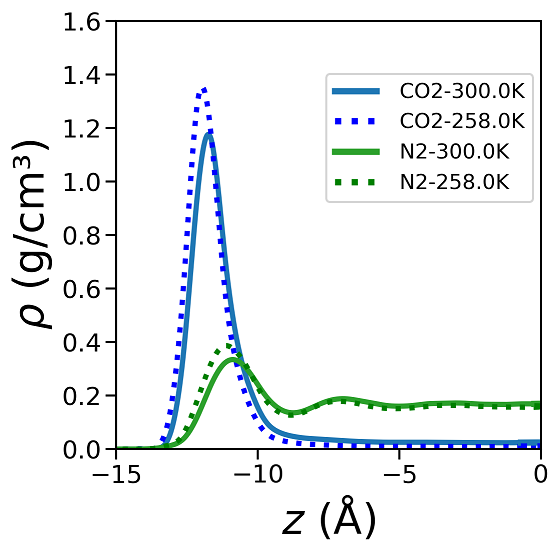
Figure 5.17: Density profiles of the CO_2 (blue) in mixtures of CO_2 + CH_4 and N_2 (green) in CH_4 + N_2 mixtures within a calcite slit-pore varying the temperature.
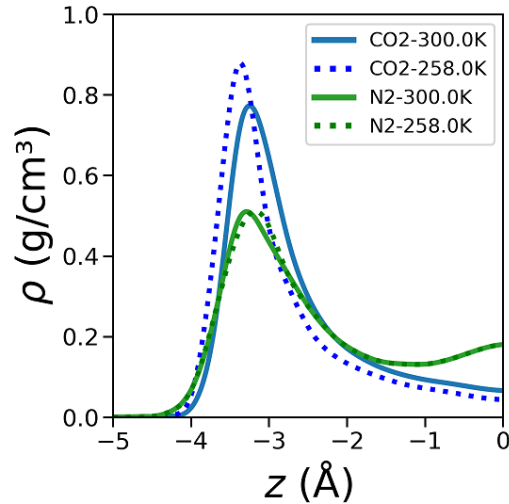
Figure 5.18: Density profiles of the CO_2 (blue) in mixtures of CO_2 + CH_4 and N_2 (green) in CH_4 + N_2 mixtures within a montmorillonite slit-pore varying the temperature.

With the reduction of 42 K, a maximum increase of 15% in the preference of components for the wall was observed, as measured by the height of the corresponding density peak. In the case of nitrogen in the mixture of N_2 + CH_4 in the montmorillonite pore (Figure 5.18), has been no change observed as a result of reduction in temperature.

In general, what was observed in this dissertation was a change in the dynamics of the mixtures of CH_4 + CO_2 and CH_4 + N_2 when they are confined in different porous rocks. We observed that fluids in nanopores are inhomogeneous in the direction perpendicular to the fluid-wall interface – in which adsorption and/or packing phenomena are observed. The influence of pore size and temperature on these effects was also analyzed.

Chapter 6

Conclusion

In this work, a series of molecular dynamics simulations was carried out in order to obtain a better understanding of the of the presence of CO_2 and N_2 in mixtures with methane inside nanopores of three different solids: montmorillonite, calcite, and barite. Calcite showed the best degree of separation for the CO_2 + CH_4 mixture. With the remaining two solids, a less significant separation is noted. The CH_4 + N_2 mixture proved to be difficult to separate through this type of adsorptive process, as expected due to literature review. The best separation for this mixture took place in barite, with nitrogen having larger density peaks closer to the wall. This result was considered interesting because no results were found in the literature on methane and nitrogen mixtures in barite nanopores. Even so, the separation can hardly be considered satisfactory, because, in the center of the pore, the two components are present in abundance. As a suggestion for future work is the more detailed study of this system and new ways to favor the separation of this mixture. It is possible to observe that, as expected, density profile in the pore is more uniformly distributed in larger pores when the load is kept unchanged, with reduction of the overall density. In addition, a reduction of temperature contributed to an increase of the adsorption of CO_2 and N_2 in most cases. This study shows that molecular dynamics can provide important information about the molecular mechanisms associated with the capture of CO_2 and N_2 in natural and complex materials. As suggestions for future work, we can mention density adjustment within the pores with real data and not idealizations, the study of other solids by means of the created protocol and the calculation of transport properties, such as viscosity

and diffusion coefficients. We can also suggest to study the pressure tensor behavior inside the pores and mechanisms to find the fluid/wall adsorption equilibrium.

Chapter 7

References

[1] MINISTÉRIO DE MINAS E ENERGIA. *E PRODUÇÃO DE PETRÓLEO E GÁS NATURAL - 2017*. Technical report, 2018.

[2] ANP. *Anuário Estatístico 2018*. Technical report, 2018. Available at: <`http://www.anp.gov.br/images/publicacoes/anuario-estatistico/2017/anuario{_}2017.pdf`>.

[3] RUFFORD, T. E., SMART, S., WATSON, G. C., et al. "The removal of CO 2 and N 2 from natural gas: A review of conventional and emerging process technologies", *Journal of Petroleum Science and Engineering*, v. 94-95, pp. 123–154, 2012. ISSN: 09204105. doi: 10.1016/j.petrol.2012.06.016. Available at: <`http://dx.doi.org/10.1016/j.petrol.2012.06.016`>.

[4] CYGAN, R. T., ROMANOV, V. N., MYSHAKIN, E. M. "Molecular simulation of carbon dioxide capture by montmorillonite using an accurate and flexible force field", *Journal of Physical Chemistry C*, v. 116, n. 24, pp. 13079–13091, 2012. ISSN: 19327447. doi: 10.1021/jp3007574.

[5] MARTIN, G. M., SIEPMANN, J. I. "Transferable Potentials for Phase Equilibria. 1. United-Atom Description of n-Alkanes", *The Journal of Physical Chemistry B*, v. 102, n. 25, pp. 2569–2577, 1998. ISSN: 1520-6106. doi: 10.1021/jp990822m.

[6] VUJIĆ, B., LYUBARTSEV, A. P. "Transferable force-field for modelling of CO2, N2, O2 and Ar in all silica and Na+ exchanged zeolites", *Modelling and Simulation in Materials Science and Engineering*, v. 24, n. 4, 2016. ISSN: 1361651X. doi: 10.1088/0965-0393/24/4/045002.

[7] CYGAN, R. T., LIANG, J.-J., KALINICHEV, A. G. "Molecular Models of Hydroxide, Oxyhydroxide, and Clay Phases and the Development of a

General Force Field", *The Journal of Physical Chemistry B*, v. 108, n. 4, pp. 1255–1266, 2004. ISSN: 1520-6106. doi: 10.1021/jp0363287. Available at: <http://pubs.acs.org/doi/abs/10.1021/jp0363287>.

[8] JANG, Y. H., CHANG, X. Y., BLANCO, M., et al. "The MSXX force field for the barium sulfate-water interface", *Journal of Physical Chemistry B*, v. 106, n. 38, pp. 9951–9966, 2002. ISSN: 10895647. doi: 10.1021/jp0133900.

[9] XIAO, S., EDWARDS, S. A., GRÄTER, F. "A new transferable forcefield for simulating the mechanics of CaCO 3 crystals", *Journal of Physical Chemistry C*, v. 115, n. 41, pp. 20067–20075, 2011. ISSN: 19327447. doi: 10.1021/jp202743v.

[10] ANP. *Boletim de recursos e reservas de petróleo e gás natural. Agência Nacional do Petróleo.* Technical report, 2018.

[11] ANP. "Resolução ANP Nº16". 2008. Available at: <http://www.scgas.com.br/uploads/editores/20100720165420.pdf>.

[12] KIDNAY, A. J., PARRISH, W. R., MCCARTNEY, D. G. *Fundamentals of Natural Gas Processing.* 2006. doi: 10.1201/b14397.

[13] SANTOS, M. S., FRANCO, L. F., CASTIER, M., et al. "Molecular Dynamics Simulation of n-Alkanes and CO2 Confined by Calcite Nanopores", *Energy and Fuels*, v. 32, n. 2, pp. 1934–1941, 2018. ISSN: 15205029. doi: 10.1021/acs.energyfuels.7b02451.

[14] RUTHVEN, D. M. "Molecular sieve separations", *Chemie-Ingenieur-Technik*, v. 83, n. 1-2, pp. 44–52, 2011. ISSN: 0009286X. doi: 10.1002/cite.201000145.

[15] RITTER, J. A., EBNER, A. D. "State-of-the-art adsorption and membrane separation processes for hydrogen production in the chemical and petrochemical industries", *Separation Science and Technology*, v. 42, n. 6, pp. 1123–1193, 2007. ISSN: 01496395. doi: 10.1080/01496390701242194.

[16] TAGLIABUE, M., FARRUSSENG, D., VALENCIA, S., et al. "Natural gas treating by selective adsorption: Material science and chemical engineering interplay", *Chemical Engineering Journal*, v. 155, n. 3, pp. 553–566, 2009. ISSN: 13858947. doi: 10.1016/j.cej.2009.09.010.

[17] BAGHERINIA, M. A., SHADMAN, M. "Investigations of CO2, CH4 and N2 physisorption in single-walled silicon carbon nanotubes using GCMC

simulation", *International Nano Letters*, v. 4, n. 1, 2014. ISSN: 2008-9295. doi: 10.1007/s40089-014-0095-6.

[18] EBNER, A. D., RITTER, J. A. *State-of-the-art adsorption and membrane separation processes for carbon dioxide production from carbon dioxide emitting industries*, v. 44. 2009. ISBN: 0149639090. doi: 10.1080/01496390902733314.

[19] FARAMAWY, S., ZAKI, T., SAKR, A. A. "Natural gas origin, composition, and processing: A review", *Journal of Natural Gas Science and Engineering*, v. 34, pp. 34–54, 2016. ISSN: 18755100. doi: 10.1016/j.jngse.2016.06.030. Available at: <http://dx.doi.org/10.1016/j.jngse.2016.06.030>.

[20] TUCKERMAN, M. E. *Statistical Mechanics: Theory and Molecular Simulations*. 1 ed. new york, Oxford University Press, 2010. ISBN: 9783540773405.

[21] THOMPSON, W. H. "Perspective: Dynamics of confined liquids", *Journal of Chemical Physics*, v. 149, n. 17, 2018. ISSN: 00219606. doi: 10.1063/1.5057759.

[22] PATHAK, M., CHO, H., DEO, M. "Experimental and Molecular Modeling Study of Bubble Points of Hydrocarbon Mixtures in Nanoporous Media", *Energy and Fuels*, v. 31, n. 4, pp. 3427–3435, 2017. ISSN: 15205029. doi: 10.1021/acs.energyfuels.6b02422.

[23] LOUGHNANE, B. J., FARRER, R. A., SCODINU, A., et al. "Dynamics of a wetting liquid in nanopores: An optical Kerr effect study of the dynamics of acetonitrile confined in sol-gel glasses", *Journal of Chemical Physics*, v. 111, n. 11, pp. 5116–5123, 1999. ISSN: 00219606. doi: 10.1063/1.479768.

[24] MORALES, C. M., THOMPSON, W. H. "Simulations of Infrared Spectra of Nanoconfined Liquids : Acetonitrile Confined in Nanoscale, Hydrophilic Silica Pores", pp. 1922–1933, 2009.

[25] WANG, S., FENG, Q., ZHA, M., et al. "Supercritical Methane Diffusion in Shale Nanopores: Effects of Pressure, Mineral Types, and Moisture Content", *Energy and Fuels*, v. 32, n. 1, pp. 169–180, 2018. ISSN: 15205029. doi: 10.1021/acs.energyfuels.7b02892.

[26] WANG, S., JAVADPOUR, F., FENG, Q. "Fast mass transport of oil and supercritical carbon dioxide through organic nanopores in shale", *Fuel*, v. 181, pp. 741–758, 2016. ISSN: 00162361. doi: 10.1016/j.fuel.2016. 05.057. Available at: <http://dx.doi.org/10.1016/j.fuel.2016.05. 057>.

[27] LE, T., STRIOLO, A., COLE, D. R. "CO2-C4H10 Mixtures Simulated in Silica Slit Pores: Relation between Structure and Dynamics", *Journal of Physical Chemistry C*, v. 119, n. 27, pp. 15274–15284, 2015. ISSN: 19327455. doi: 10.1021/acs.jpcc.5b03160.

[28] LE, T. T. B., STRIOLO, A., GAUTAM, S. S., et al. "Propane-Water Mixtures Confined within Cylindrical Silica Nanopores: Structural and Dynamical Properties Probed by Molecular Dynamics", *Langmuir*, v. 33, n. 42, pp. 11310–11320, 2017. ISSN: 15205827. doi: 10.1021/acs.langmuir. 7b03093.

[29] FRANCO, L. F., CASTIER, M., ECONOMOU, I. G. "Anisotropic parallel self-diffusion coefficients near the calcite surface: A molecular dynamics study", *Journal of Chemical Physics*, v. 145, n. 8, 2016. ISSN: 00219606. doi: 10.1063/1.4961408. Available at: <http://dx.doi.org/10.1063/ 1.4961408>.

[30] KARRA, J. R., WALTON, K. S. "Molecular Simulations and Experimental Studies of CO2, CO, and N2 Adsorption in Metal-Organic Frameworks", *J. Phys. Chem. C*, v. 114, pp. 15735–15740, 2010. doi: 10.1021/jp105519h.

[31] MISHRA, P., MEKALA, S., DREISBACH, F., et al. "Adsorption of CO2, CO, CH4 and N2 on a zinc based metal organic framework", *Separation and Purification Technology*, v. 94, pp. 124–130, 2012. ISSN: 13835866. doi: 10.1016/j.seppur.2011.09.041. Available at: <http://dx.doi.org/10. 1016/j.seppur.2011.09.041>.

[32] ZHANG, Z., LI, Z., LI, J. "Computational Study of Adsorption and Separation of CO2 and CH4 and N2 by an rht-Type Metal−Organic Framework.pdf", *Langmuir*, v. 28, pp. 12122–12133, 2012.

[33] YI, H., LI, F., NING, P., et al. "Adsorption separation of CO 2 , CH 4 , and N 2 on microwave activated carbon", *Chemical Engineering Journal*, v. 215-216, pp. 635–642, 2013. ISSN: 13858947. doi: 10.1016/j.cej.2012.11.050. Available at: <http://dx.doi.org/10.1016/j.cej.2012.11.050>.

[34] BILLEMONT, P., COASNE, B., WEIRELD, G. D. "Adsorption of Carbon Dioxide, Methane, and Their Mixtures in Porous Carbons: Effect of Surface Chemistry, Water Content, and Pore Disorder", 2013.

[35] AKBARZADEH, H., ABBASPOUR, M. "A comprehensive study of methane/carbon dioxide adsorptive selectivity in different bundle nanotubes", *RSC Advances*, v. 6, n. 74, pp. 69845–69854, 2016. ISSN: 20462069. doi: 10.1039/c6ra16672e. Available at: <`http://dx.doi.org/10.1039/C6RA16672E`>.

[36] DANG, Y., ZHAO, L., LU, X., et al. "Molecular simulation of CO 2 /CH 4 adsorption in brown coal: Effect of oxygen-, nitrogen-, and sulfur-containing functional groups", *Applied Surface Science*, v. 423, pp. 33–42, 2017. ISSN: 01694332. doi: 10.1016/j.apsusc.2017.06.143. Available at: <`http://dx.doi.org/10.1016/j.apsusc.2017.06.143`>.

[37] BACSIK, Z., ATLURI, R., GARCIA-BENNETT, A. E., et al. "Temperature-induced uptake of CO 2 and formation of carbamates in mesocaged silica modified with n-propylamines", *Langmuir*, v. 26, n. 12, pp. 10013–10024, 2010. ISSN: 07437463. doi: 10.1021/la1001495.

[38] BLEIWAS, D. I., MILLER, M. M. "Barite—A Case Study of Import Reliance on An Essential Material for Oil and Gas Exploration and Development Drilling", *Geological Survey Scientific Investigations Report*, v. 2014-5230, pp. 1–14, 2015.

[39] FRENKEL, D.; SMIT, B. *Understanding Molecular Simulation*. Academic Press: New York, 2002.

[40] VERLET, L. "\href{https://journals.aps.org/pr/pdf/10.1103/PhysRev.159.98}{Computer Experiments on Classical Fluids. I. Thermodynamical Properties of Lennar-Jones Molecules}", *Physical Review*, v. 159, n. 1, pp. 98–103, 1967. doi: 10/b4fphb. Available at: <`https://journals.aps.org/pr/pdf/10.1103/PhysRev.159.98`>.

[41] SWOPE, W. C., ANDERSEN, H. C., BERENS, P. H., et al. "A computer simulation method for the calculation of equilibrium constants for the formation of physical clusters of molecules: Application to small water clusters", *The Journal of Chemical Physics*, v. 76, n. 1, pp. 637–649, 1982. ISSN: 00219606. doi: 10.1063/1.442716.

[42] MARTYNA, G. J., TUCKERMAN, M. E., TOBIAS, D. J., et al. "Explicit reversible integrators for extended systems dynamics", *Molecu-

lar Physics, v. 87, n. 5, pp. 1117–1157, 1996. ISSN: 13623028. doi: 10.1080/00268979600100761.

[43] WILLIAM G. HOOVER. "Canonical dynamics: Equilibrium phase-space distributions William", *Physical Review A*, v. 31, n. 4, pp. 1695–1697, 1985. ISSN: 01728083. doi: 10.1007/BF00419952.

[44] HANWELL, M. D., CURTIS, D. E., LONIE, D. C., et al. "Avogadro: An advanced semantic chemical editor, visualization, and analysis platform", *Journal of Cheminformatics*, v. 4, n. 8, 2012. ISSN: 17582946. doi: 10.1186/1758-2946-4-17.

[45] ABREU, C. R. A. "Playmol". `https://github.com/atoms-ufrj/playmol`, 2018.

[46] JONES, L. "On the Determination o f Molecular Fields. — II. From the Equation o f State o f a Gas." v. 4, n. 71, 1924.

[47] MIE, G. "Zur kinetischen Theorie der einatomigen Körper", *Annalen der Physik*, v. 316, n. 8, pp. 657–697, 1903. ISSN: 15213889. doi: 10.1002/andp.19033160802.

[48] STEVE PLIMTON. "Fast Parallel Algorithms for Short-Range Molecular Dynamics", *Journal of Computational Physics*, v. 117, n. 1, pp. 1–19, 1995. ISSN: 00219991. doi: https://doi.org/10.1006/jcph.1995.1039. Available at: <`http://www.cs.sandia.gov/\protect$\relax\sim$sjplimp/main.html`>.

[49] MARTYNA, G. J., KLEIN, M. L., TUCKERMAN, M. "Nosé-Hoover chains: The canonical ensemble via continuous dynamics", *The Journal of Chemical Physics*, v. 97, n. 4, pp. 2635–2643, 1992. ISSN: 00219606. doi: 10.1063/1.463940.

[50] HOCKNEY, R. W., EASTWOOD, J. W. *Computer Simulation Using Particles*. 1988. doi: 10.1887/0852743920.

[51] BOŢAN, A., ROTENBERG, B., MARRY, V., et al. "Hydrodynamics in clay nanopores", *Journal of Physical Chemistry C*, v. 115, n. 32, pp. 16109–16115, 2011. ISSN: 19327447. doi: 10.1021/jp204772c.

[52] ZHANG, Q., LIU, R., PANG, Z., et al. "Characterization of microscopic pore structures in Lower Silurian black shale(S1l), southeastern Chongqing, China", *Marine and Petroleum Geology*, v. 71, pp. 250–259, 2016. ISSN:

02648172. doi: 10.1016/j.marpetgeo.2015.12.015. Available at: <http://dx.doi.org/10.1016/j.marpetgeo.2015.12.015>.

[53] LEONI, F., FRANZESE, G. "Effects of confinement between attractive and repulsive walls on the thermodynamics of an anomalous fluid", *Physical Review E*, v. 94, n. 6, pp. 1–11, 2016. ISSN: 24700053. doi: 10.1103/PhysRevE.94.062604.

[54] SALGADO-BLANCO, D., MENDOZA, C. I., CHÁVEZ-ROJO, M. A., et al. "Influence of anchoring in the phase behaviour of discotic liquid crystals", *Soft Matter*, v. 14, n. 15, pp. 2846–2859, 2018. ISSN: 17446848. doi: 10.1039/c7sm02311a.

[55] AIMOLI, C. G., MAGINN, E. J., ABREU, C. R. A. "Thermodynamic Properties of Supercritical Mixtures of Carbon Dioxide and Methane: A Molecular Simulation Study", *Journal of Chemical & Engineering Data*, v. 59, n. 10, pp. 3041–3054, 2014. ISSN: 0021-9568. doi: 10.1021/je500120v. Available at: <http://pubs.acs.org/doi/abs/10.1021/je500120v>.